Bulletin of the Seismological Society of America, Vol. 101, No. 1, pp. 313–326, February 2011, doi: 10.1785/0120100063

Stress and Seismicity Changes on the Sunda Megathrust Preceding the 2007 M_w 8.4 Earthquake

by Kelly Wiseman and Roland Bürgmann

Abstract The Bengkulu M_w 8.4 earthquake on 12 September 2007, close in time and space to the 2004 M_w 9.2 Sumatra–Andaman and 2005 M_w 8.7 Nias megathrust events, suggests that it could be a triggered earthquake. It was located in the southern portion of the historic 1833 M_w 8.9 rupture. However, it appears perplexing that the portion of the Sunda subduction zone between the Nias and Bengkulu rupture patches, which last ruptured in a 1797 M_w 8.7 event, did not recur first. Coulomb failure stress (CFF) modeling of the 2004 and 2005 megathrust earthquakes and subsequent post-seismic relaxation processes fails to explain why the 2007 patch ruptured before the northern 1797 segment. Surprisingly, the much smaller 2000 M_w 8.0 Enggano earthquake produced a much larger positive CFF change at the 2007 hypocenter and may help to explain the southern location of the 2007 earthquake. Investigation of changes in seismicity rates in the region following the 2004–2005 events shows that the megathrust earthquakes may have dynamically triggered slip near the northern end of the 2007 rupture zone. A large increase in seismicity levels following the 2000 earthquake may also have influenced the eventual initiation point of the 2007 earthquake. Regrettably, the section of the Sunda megathrust near Siberut that last ruptured in 1797 still poses a great seismic hazard to the region as the only segment not to have ruptured in the sequence of twenty-first century megathrust earthquakes.

Online Material: Stress change models and seismicity rate change maps.

Introduction

The 2004 M_w 9.2 Sumatra–Andaman earthquake was the largest in 40 yr and extended for 1300–1500 km (e.g., Shearer and Bürgmann, 2010). It apparently triggered a second great megathrust event, the 28 March 2005 M_w 8.7 Nias earthquake, which initiated just ~200 km south of the 2004 epicenter (McCloskey *et al.*, 2005; Nalbant *et al.*, 2005; Pollitz, Banerjee, *et al.*, 2006). Earthquake triggering is the process by which static and/or dynamic stress changes associated with an earthquake can induce or retard seismic activity in the surrounding region or trigger other earthquakes at great distances (Freed, 2005 and references therein). The 12 September 2007 Bengkulu M_w 8.4 earthquake initiated ~750 km south of the 2005 epicenter, and was followed 12 hr later by a deeper M_w 7.9 aftershock (Figs. 1, 2a). Their occurrence, close in time and space to the 2004 Sumatra–Andaman earthquake, the 2005 Nias earthquake, and the 2000 M_w 8.0 Enggano earthquake, suggest the possibility of these being triggered events.

The 2007 earthquakes ruptured a portion of the 700-km-long Mentawai patch, a section of the Sunda megathrust that has been observed to fail in sequences of earthquakes about every two centuries for the past 700 yr (Sieh *et al.*, 2008). The last earthquake supercycle ended in a pair of $M8+$ events in 1797 and 1833. The 1797 earthquake ruptured directly south of the 2005 Nias rupture patch, which apparently also slipped in 1861, while the 1833 segment is farther south and overlaps with the 2007 events (Fig. 1). The study of coral growth histories offshore Sumatra by Natawidjaja *et al.* (2006) indicates that interseismic strain accumulated along the 1833 segment has approached levels relieved in the historic earthquake. In addition, the accumulated interseismic strain appears to have exceeded previously relieved levels along the 1797 segment (Chlieh *et al.*, 2008). Although there are moment magnitude uncertainties ranging from 0.2 to 0.3 for the historic 1797 and 1833 source models, historic reports and coral microatoll data indicate that the 1833 rupture was larger, along with being the more recent event, and should therefore rerupture after the 1797 segment.

Previous investigations of coseismic and viscoelastic deformation following the 2004–2005 sequence show that the 1797 segment experienced higher Coulomb failure stress increases (CFF) than the more distant 1833 segment (Nalbant *et al.*, 2005; Pollitz, Banerjee, *et al.*, 2006). Therefore,

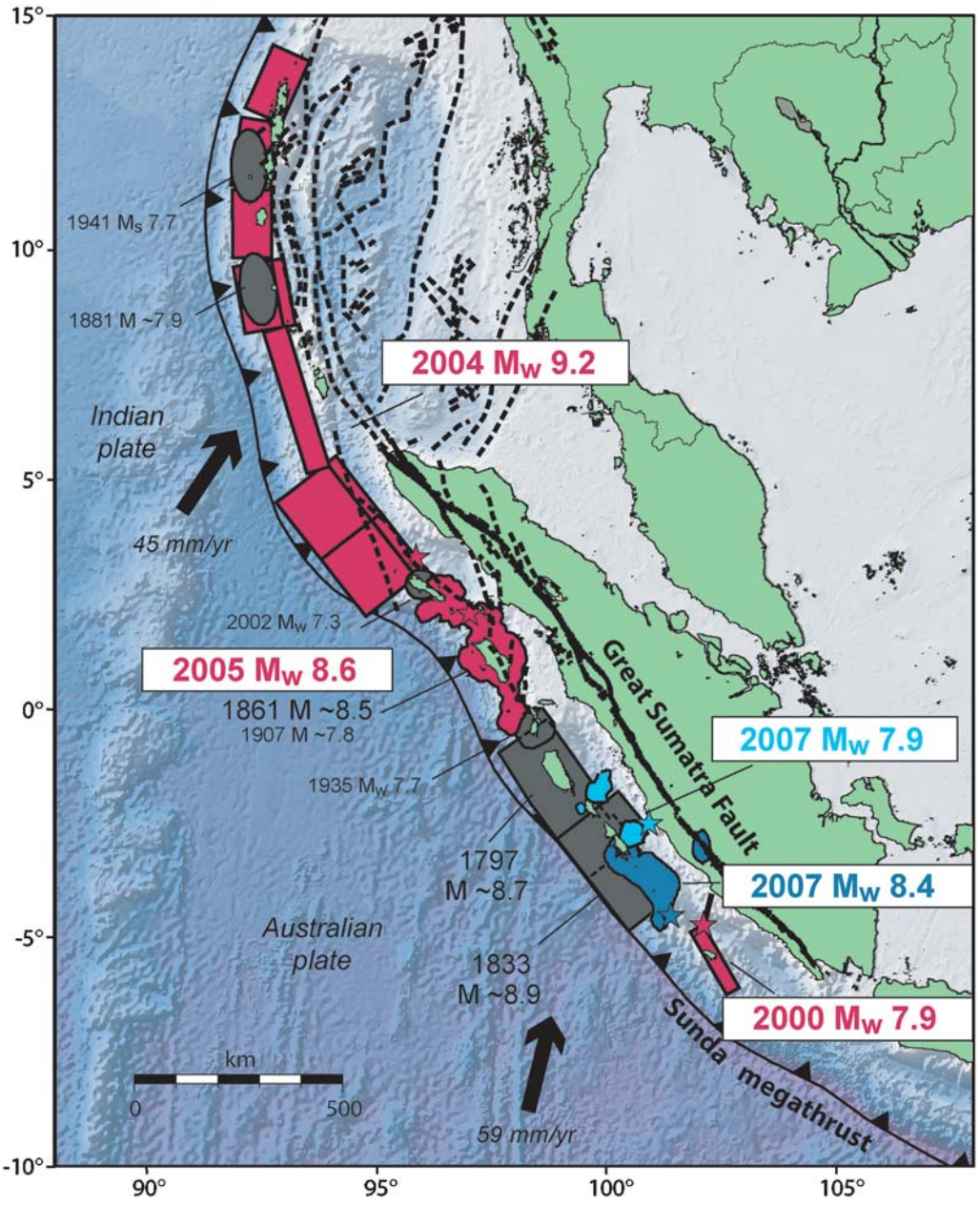

Figure 1. Tectonic overview of the Sunda subduction zone. Rupture patches and estimated magnitudes from recent great earthquakes are from Abercrombie *et al.* (2003), Banerjee *et al.* (2007), and Konca *et al.* (2007) and historic earthquakes are from Briggs *et al.* (2006) and Natawidjaja *et al.* (2006). High-slip patches from the 2007 M_w 8.4 and M_w 7.9 events are from Konca *et al.* (2008).

assuming that the stress distribution at the time of these events was relatively uniform, it is unclear why the 1797 and northern portion of the 1833 rupture zone did not break before the southern 1833 segment. We model stress changes from coseismic and postseismic processes, including viscoelastic relaxation, afterslip, and poroelastic rebound, in an attempt to find scenarios that can explain why the southern 1833 segment was triggered prior to the 1797 segment. In addition, we investigate the seismicity changes in the years leading up to the 2007 earthquake for alternative triggering evidence.

Stress Modeling Method and Data

Coseismic and Postseismic Deformation Calculations

We model the coseismic and postseismic deformation from the 2000, 2004, and 2005 earthquakes, constrained by geodetic and seismological observations (Abercrombie *et al.*, 2003; Pollitz, Bürgmann, and Banerjee, 2006, Hsu *et al.*, 2006; Banerjee *et al.*, 2007; Konca *et al.*, 2007; Pollitz *et al.*, 2008), in order to quantify the associated stress changes in the hypocentral region of the 2007 earthquake. The elastic coseismic deformation is calculated in a layered

spherical geometry using the direct Greens function method of Pollitz (1996). We also use this method to model the cumulative elastic deformation from the aseismic afterslip observed after the 2004–2005 earthquake sequence (Hsu *et al.*, 2006; Banerjee *et al.*, 2007; Chlieh *et al.*, 2007). The elastic structure of the Earth is based on the seismically determined global Earth model PREM (Dziewonski and Anderson, 1981).

Deep-seated transient postseismic relaxation can produce time-dependent deformation and stress changes, exceeding those from the earthquake itself in the intermediate-to-far-field range. The 2004–2005 earthquake sequence produced large stress increases downdip from the coseismic rupture zone, which are expected to drive viscoelastic relaxation of the low-viscosity asthenosphere. A number of studies have examined the viscoelastic relaxation resulting from the 2004 earthquake for the year following the event (e.g. Pollitz, Banerjee, *et al.*, 2006; Pollitz, Bürgmann, and Banerjee, 2006; Pollitz *et al.*, 2008), but we extend our model to the time of the 2007 earthquake. Postseismic deformation resulting from the viscoelastic relaxation is calculated on a layered, laterally homogeneous, spherical earth using the method of Pollitz (1992). This method sums viscoelastic normal modes from earthquake excitation. We employ the oceanic rheology model of Pollitz, Bürgmann, and Banerjee (2006) that fits the initial horizontal postseismic velocity, and the GPS time-series, between the 2004 and 2005 events. This model includes a bi-viscous asthenosphere with an initial short-term viscosity of 5×10^{17} Pa s and a long-term viscosity of 1×10^{19} Pa s. We extend the elastic lid to 80 km depth in accordance with the potentially deep, isolated 2007 M_w 8.4 rupture patch (Konca *et al.*, 2008).

The strain field resulting from a coseismic dislocation produces changes in pore-fluid-pressure in the brittle upper crust. The subsequent decay of the excess pore-fluid-pressure gradients will lead to fluid flow and poroelastic deformation. Masterlark *et al.* (2001) and Masterlark (2003) have previously modeled the effects of poroelastic rebound in a subduction setting and demonstrated that poroelastic effects are generally only significant in the near field directly surrounding the rupture area. We approximate the fully relaxed poroelastic response by subtracting the undrained solution for coseismic deformation from the drained solution for coseismic deformation. Based on the Fialko (2004) study of poroelastic rebound following the 1992 Landers strike-slip earthquake and the Masterlark (2003) study of the 1995 Jalisco–Colima subduction zone earthquake, the crust is assumed to be fluid-saturated down to ~15 km depth. Ogawa and Heki (2007) propose that the downgoing slab releases fluids into the mantle wedge in sufficiently high quantities, with sufficiently large pore pressure diffusivities, to contribute to the poroelastic rebound during the early postseismic period. We therefore test a range of earth models, with undrained Poisson's ratio values 0.05 above the drained value for the top 15 km, 30 km, and 60 km of the lithosphere.

Input Source Models

For our coseismic and postseismic deformation calculations, we use previously derived slip distributions based on geodetic and seismological data. For the 2004 Sumatra–Andaman earthquake, we use the GPS-based slip model by Banerjee *et al.* (2007). The coseismic slip model includes 15 rupture patches from 0 to 50 km depth with a maximum of ~19 m of slip. In a few places where sufficient near-field measurements were made following the 2004 earthquake, rapidly decaying deep afterslip can be resolved (e.g., Banerjee *et al.*, 2007; Paul *et al.*, 2007). We consider a simple afterslip model that includes 1 m of slip over the 30- to 50-km depth coseismic rupture patches and over a 50- to 60-km depth extension downdip of the coseismic rupture patches.

For the Nias earthquake, we adapt the slip model from Konca *et al.* (2007), which is based on continuous GPS (cGPS), seismic, and coral data. We discretize their slip model into 35 segments, ranging from 4 to 59 km depth. The maximum slip is ~15 m at 27 km depth. In addition, Hsu *et al.* (2006) and Prawirodirdjo *et al.* (2010) observed significant afterslip updip and downdip from the main Nias rupture. For our modeling purposes, we logarithmically extend the 9-month afterslip distribution from Hsu *et al.* (2006) to the time of the 2007 earthquake.

Along with the 2004–2005 megathrust sequence, we also consider the smaller 2000 Enggano M_w 8.0 earthquake, which ruptured to the south of the 2007 epicenter. This earthquake is not as well constrained as the later sequence, but is reported to be primarily a left-lateral strike-slip event in the downgoing Australian plate (Zhou *et al.*, 2002; Abercrombie *et al.*, 2003). Zhou *et al.* (2002) uses teleseismic body waves to estimate a 95-km-long, 60-km-wide rupture area with an average slip of 11 m. Abercrombie *et al.* (2003) find that the rupture was comprised of two subevents. The predominant strike-slip component released ~65% of the moment and triggered a thrust subevent on the plate-interface (Fig. 2a). Most of the Enggano aftershocks are located to the southeast of the mainshock and are consistent with the rupture area of the thrust subevent (Fig. 2b). The aftershock catalog shows a diversity of mechanisms, also consistent with a two-subevent model. Therefore, we use the Abercrombie *et al.* (2003) solution as our preferred slip model. For the rupture area, we took the average values of the along-strike length ranges given for the two subevents, 75 km and 175 km, respectively. Since there were no aftershocks in the top ~15 km of the crust, we assume that the downdip extent of the rupture was from the 57-km-deep hypocenter up to 15 km depth. Given a moment of 1.23×10^{21} Nm, the strike-slip subevent had an average of 4 m of slip, and the thrust subevent had 1 m of slip.

Coulomb Failure Stress-Change Calculations

The deformation calculations are used as input to model the CFF changes along the Sunda megathrust. Previous studies have shown that CFF increases of 100–300 kPa are generally

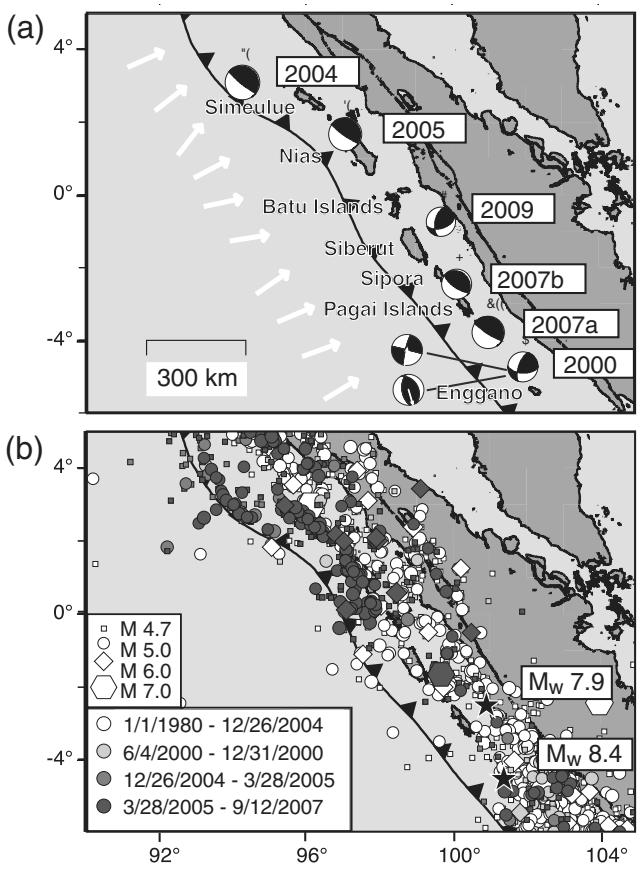

Figure 2. (a) Location of Indonesian islands mentioned in the text and focal mechanisms for the recent great earthquakes (Global CMT catalog). The two-subevent focal mechanisms for the 2000 earthquake are also included (Abercrombie *et al.*, 2003). The slip-vector orientations used in the CFF models are shown with arrows. (b) Earthquake epicenters, sized by magnitude and shaded by time period, for events along the Sunda subduction zone (see text for earthquake catalog description).

capable of triggering seismicity, and it has been suggested that even tens of kPa are sufficient to advance (or retard) the occurrence of large earthquakes (e.g., Rydelek and Sacks, 1999; Lin and Stein, 2004). Toda *et al.* (2005) suggested that CFF calculations, in combination with knowledge of the background seismicity rate, could even be used as an earthquake forecasting tool. Due to a lack of knowledge of the total stress field on the Sunda megathrust, and the nonlinear nature of the earthquake triggering process, the use of CFF calculations in forecasting has its limits. However, retrospectively analyzing earthquakes using the CFF method helps to sharpen our limited forecasting skills by better understanding the levels of stress necessary to initiate an earthquake.

We use a CFF function given by $\Delta\mathrm{CFF} = \Delta\tau + \mu'\Delta\sigma_n$, which defines ΔCFF as a sum of the change in shear stress τ and the change in normal stress (clamping is negative) σ_n multiplied by an effective coefficient of friction. We assume low frictional fault strength and use an effective coefficient of friction, $\mu' = 0.1$. This is comparable to friction estimates in the studies by Wang *et al.* (1995) and Wang and He (1999), which found the Cascadia subduction zone to be very weak and to basal detachment frictional strengths inferred from accretionary wedge tapers (Suppe, 2007).

Megathrust Geometry

The previously mentioned coseismic slip distributions all use different geometric parameters for their rupture planes. The CFF changes are resolved onto the Sunda megathrust, and variation in the dip, rake, and strike of the source ruptures and receiver geometry can affect the results. Figure 3 shows the receiver fault geometry on which we calculate stress changes. The megathrust geometry follows the strike of the Sunda trench (Curray, 2005). We choose a downward steepening geometry that represents a compromise between the published megathrust geometries of Subarya *et al.* (2006) and Chlieh *et al.* (2008). These two studies fit a curved megathrust surface based on hypocenter locations and the dip angle indicated by interplate earthquake focal mechanisms. Published source and megathrust fault geometries vary by as much as 25°. The stress calculations are most sensitive to geometrical differences near the downdip and updip ends of the high-slip zones. For example, when comparing CFF changes from the 2004 earthquake resolved on both planar and curved plate geometries, the stress-change magnitudes vary by up to a factor of 3 on the subduction thrust below the Sumatran forearc islands due to their proximity to the downdip edge of the 2004 rupture patch (Table 1). However, such variations in geometry insubstantially impact the calculated stress-change values on the deeper portions of the megathrust, at depths greater than the source model (for CFF change maps using variable fault geometry, Ⓔ see Fig. S1 in the electronic supplement to this paper).

Our preferred slip-vector rakes on the receiver fault are based on fault plane parameters for earthquake mechanisms obtained from the Global Centroid Moment Tensor Project (see the Data and Resources section). We filtered the catalog for plate-interface events by restricting the catalog to fault planes with a strike in the range of 280° to 360°, dip in the range of 0° to 35°, and rake in the range of 80° to 130°.

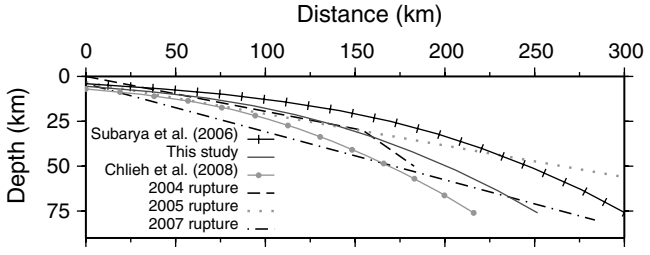

Figure 3. Sunda plate-interface geometry comparison. The solid line shows our preferred megathrust geometry, intermediate to the geometries used in Subarya *et al.* (2006) and Chlieh *et al.* (2008). The geometry of the southernmost 2004 rupture segment (Banerjee *et al.*, 2007), the 2005 rupture (Konca *et al.*, 2007), and the preferred dip of the two 2007 ruptures (Konca *et al.*, 2008) are also plotted.

Table 1
2004 Averaged Coseismic CFF Changes under the Sumatran Forearc Islands (kPa)

Megathrust Geometry	Simeulue	Nias	Batu Islands	Siberut
Curved interface	245	22	6	2
10° dip	250	30	5	2
15° dip	220	12	2	< 1
20° dip	205	9	2	< 1

This restricted the catalog to 377 events, which we then separated into 1° latitude bins and used their average rake. The rake varies between 95° and 108° (Fig. 2a).

Stress Modeling Results

Interseismic Loading Rate

In order to ascertain the relevance of the coseismic and postseismic stresses induced by the megathrust earthquakes, it is important to first calculate the interseismic loading rate. The interseismic loading rate is dependent on the plate convergence rate and the locking depth, which Chlieh *et al.* (2008) has shown to be considerably heterogeneous along the Sunda megathrust. They use a backslip approach to determine the heterogeneous coupling model that best fits their compilation of paleogeodetic and geodetic data. The coupling on the Sunda megathrust between the Pagai Islands and Enggano is not well constrained, as there are large differences between the forward and inverse models of Chlieh *et al.* at these latitudes. Their preferred forward model has the megathrust locked between the trench and approximately 40 km depth at the latitude of the 2007 hypocenter, and provides an upper bound on the level of locking for this portion of the megathrust. We determine the static stress drop due to the accumulated moment deficit on a rectangular dip-slip fault (Aki, 1966) in order to get an average interseismic loading rate. This interseismic loading rate, of 26 kPa/yr, is an average value for the portion of the plate-interface from the trench to the 40-km locking depth.

We compared this average tectonic loading rate based on the backslip approach with loading due to a buried fault downdip of the 2007 rupture. The buried plate-interface fault starts at the 40-km locking depth and extends to a depth of 600 km. We use a two-segment planar fault model, with the upper segment extending from 40 km to 110 km at a 30° dip and the lower plane extending from 110 km to 600 km at a 40° dip (for representation of interseismic planar fault model, Ⓔ see Fig. S2a in the electronic supplement to this paper). We impose 4.5 cm/yr of pure reverse slip on the buried faults, based on the long-term convergence rate between the forearc sliver and the Australian plate (Chlieh *et al.*, 2008). This method leads to a heterogeneous loading of the megathrust, with maximum stresses concentrated at the boundary between the locked and sliding portion of the plate-interface (for cross sections of interseismic changes, Ⓔ see Fig. S2b,c, d in the electronic supplement to this paper). Based on the buried fault approach, the interseismic loading rate at the hypocentral depth of the 2007 earthquake is 5 kPa/yr.

Stress Change from the 2004 Sumatra–Andaman Earthquake

The broad patterns of the modeled CFF change are large stress decreases (i.e., stress drop) over the ruptured region, large stress increases both updip and downdip of the coseismic slip patches, and moderate stress increases past the southern edge of the ruptured region (Fig. 4a). As shown in previous studies (e.g., Gahalaut, 2005; Nalbant *et al.*, 2005; Pollitz, Banerjee, *et al.*, 2006), the future Nias hypocenter was substantially stressed by the 2004 coseismic deformation. The magnitude of the CFF change at the Nias hypocenter is very sensitive to how far south one extends the 2004 slip model and at what depth one calculates the stress. Previously published results have ranged from ~10 to 100 kPa, and have considered hypocenter depths between 10 to 40 km. When resolving the CFF on the Sunda megathrust surface, we find positive stress changes to be focused over the eventual Nias high-slip region (green contours in Fig. 4a). The 2005 hypocenter is located at 24 km depth using our preferred geometry, with a 49 kPa CFF change. The magnitude of the CFF change varies between 49 to 78 kPa between 24 km depth to the USGS hypocentral depth of 30 km, with an average of 64 kPa CFF change. The coseismic CFF change is particularly high at the 2005 hypocenter because our 2004 source model has a high-slip segment that truncates at 30 km depth. In addition, the elastic properties in our earth model have major increases in stiffness at 15-km and 25-km depth, which causes the CFF change to likewise increase at those depth intervals. However, the positive CFF change decreases rapidly alongstrike, and is < 10 kPa before it reaches the 2007 rupture zone. There is no significant CFF decrease over the northern 1797 slip segment to explain why the 2007 earthquake failed to initiate in this region.

Afterslip following the 2004 earthquake increases and expands the coseismic rupture and associated stress changes. Based on our simple afterslip model, with 1 m of slip on planes overlapping and downdip of the coseismic rupture patches, the farthest extent of the > 10 kPa CFF change is the southern edge of Simeulue Island (Fig. 4b). The CFF change at the 2005 hypocenter is 2 kPa, while the CFF change at the 2007 hypocenter is much less than 1 kPa. It is possible and even likely that small amounts of afterslip closer to the 2005 hypocenter would have produced substantially greater stress changes at this eventual earthquake initiation point. The analysis of geodectic data by Prawirodirdjo *et al.* (2010) during the year following the 2005 earthquake places up to 8 m of slip updip of the 2004 rupture, between approximately 3.5° N and 6° N. Even with this proposed large amount of afterslip, approaching the amount of slip on the southernmost coseismic rupture segment, the CFF change

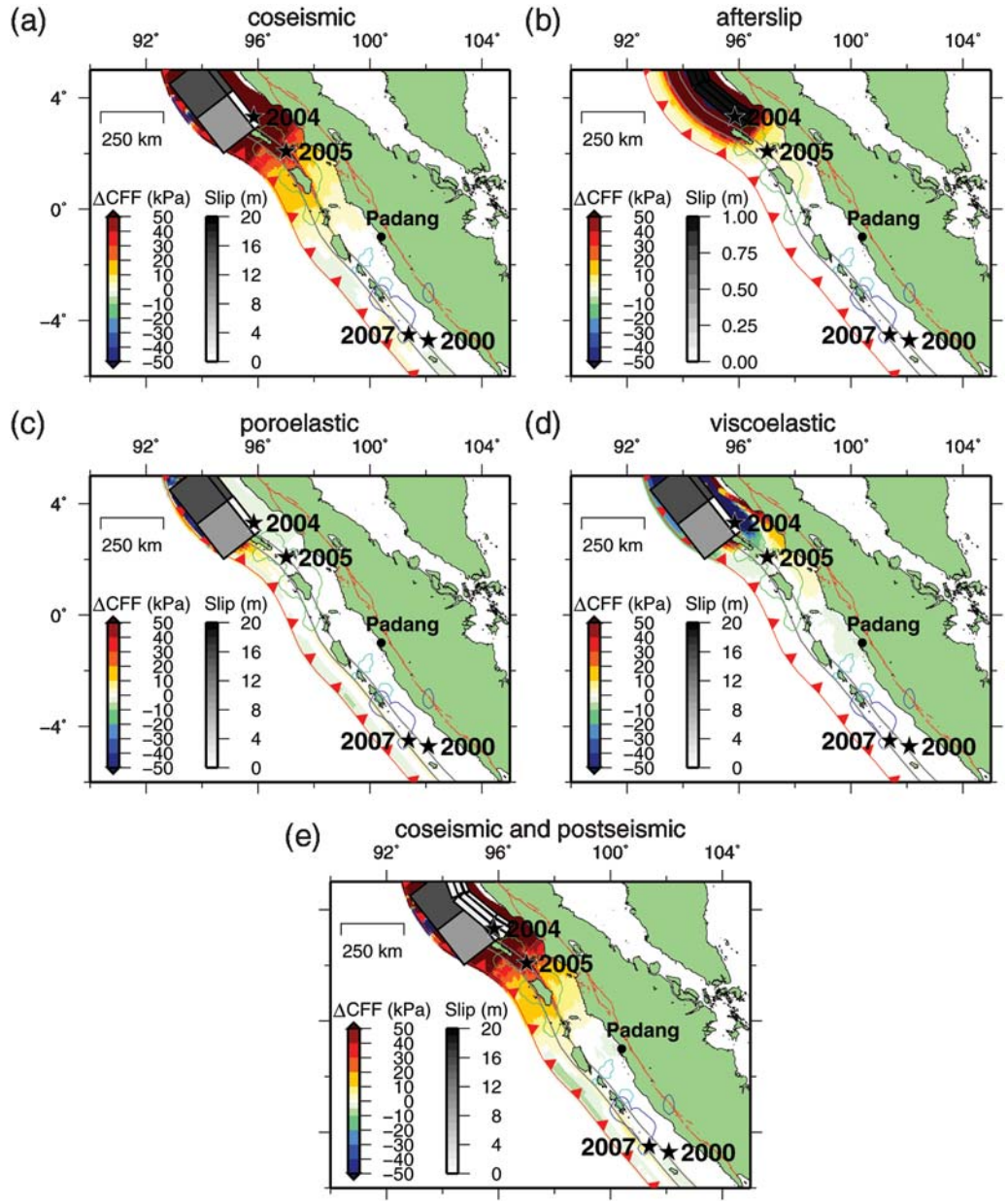

Figure 4. Coulomb failure stress changes on the Sunda megathrust resulting from the 2004 (a) coseismic deformation, (b) afterslip deformation from slip on planes at 30–60 km depth—note the smaller slip scale, (c) poroelastic deformation (with top 15 km of lithosphere fluid-saturated), (d) viscoelastic deformation, (e) total coseismic and postseismic deformation. The earthquake source model overlays the stress changes (Banerjee *et al.*, 2007). The stress changes are also overlain by the M_w 8.7 2005 5-m slip contour (Konca *et al.*, 2007), the M_w 8.4 2007 1-m slip contour, and the M_w 7.9 2007 1-m slip contour (Konca *et al.*, 2008). The major increases in elastic moduli, at 15-km and 25-km depth, are marked with gray lines on the megathrust.

would still be less than < 10 kPa over the 2007 rupture zone. More analysis of geodetic data from the time of the 2004 earthquake until the 2007 earthquake is needed to accurately constrain the total aseismic slip following the 2004 earthquake, but it likely did not substantially impact the stress field near the 2007 hypocenter.

The poroelastic effects from the 2004 event are restricted to the shallow portions of the megathrust, updip from the main coseismic slip patch. Figure 4c shows that there are no large stress changes in the along-strike direction toward the 2007 epicentral region for poroelastic rebound down to 15 km depth. Postseismic poroelastic stress changes from models with variable depths to which fluid flow occurs, ranging from 15 to 60 km, produce CFF changes that are less than 4 kPa everywhere on the 2007 rupture zone.

Viscoelastic relaxation tends to counteract the coseismic stress changes near the rupture patches. Figure 4d shows that there are positive CFF changes on the lower half of the coseismic slip segments, at approximately 15 to 40 km depth, and negative CFF changes in the surrounding region. Large

positive CFF in the shallow portion of the megathrust only extends as far south as central Simeulue Island.

Although the 2004 earthquake was an M_w 9.2 event, the ~950 km separation distance prevented the coseismic and postseismic CFF changes at the 2007 hypocenter from being > 10 kPa (Fig. 4e). As shown in previous subduction zone studies (e.g., Lin and Stein, 2004; Goldfinger *et al.*, 2008), this study highlights the fact that megathrust ruptures such as the 2004 Sumatra–Andaman earthquake load the plate-interface updip and downdip of the main rupture and adjacent nearby faults much more than faults further along-strike.

Stress Change from the 2005 Nias Earthquake

The 2005 earthquake was also too far north to produce large coseismic and postseismic CFF changes at the 2007 hypocenter (Fig. 5d) with total stress changes of < 1 kPa. However, Figure 5a shows that the coseismic CFF is > 10 kPa beneath and to the east of Siberut Island, stressing the northern 1797 rupture zone. The CFF change resulting from postseismic afterslip is shown in Figure 5b. The CFF > 10 kPa from afterslip extends to the southern edge of the Batu Islands, while substantial CFF increase from viscoelastic relaxation only reaches the northern tip of the islands (Fig. 5c). If one assumes that only the top 15 km of the lithosphere are saturated with fluids, the poroelastic CFF change of > 10 kPa is restricted to the top ~10 km of the megathrust down to 0.5° S. If the lithosphere were saturated with fluids down to 30 km depth, then the poroelastic rebound would lead to a negative CFF change below the Batu Islands.

Stress Change from the 2000 Enggano Earthquake

The largest contributor to positive CFF change at the 2007 hypocenter was the M_w 8.0 2000 earthquake (Fig. 6). The coseismic CFF change at the 2007 hypocenter is 18 kPa, a factor of 3 times larger than the interseismic loading rate at that depth. For the case of only the top 15 km being fluid-saturated, there was only a small contribution of up to ~1 kPa from poroelastic rebound because the 2000 earthquake rupture occurred below 15 km depth. Our models that assumed the lithosphere is fluid-saturated down to 30 km and 60 km depth did increase the range of high CFF changes beyond the 2000 rupture zone, but the 2007 hypocenter is too far away to be sensitive to these changes (for CFF change maps from poroelastic deformation with top 15 km, 30 km, and 60 km of lithosphere fluid-saturated, Ⓔ see Fig. S3 in the electronic supplement to this paper). Seven years of

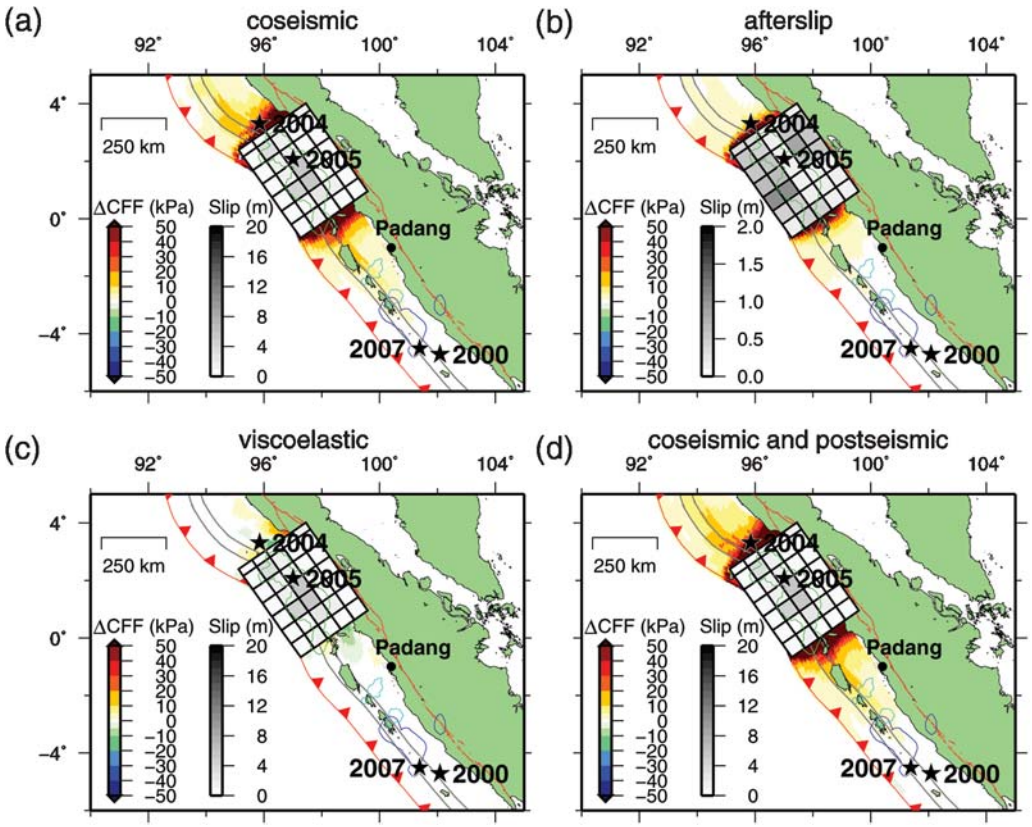

Figure 5. Coulomb failure stress changes on the Sunda megathrust resulting from the 2005 (a) coseismic deformation, (b) afterslip deformation—note the smaller slip scale, (c) viscoelastic deformation, (d) total coseismic and postseismic (including poroelastic) deformation. The 2005 earthquake source models (Hsu *et al.*, 2006; Konca *et al.*, 2007) and 2007 slip contours overlay the stress changes (Konca *et al.*, 2008). The major increases in elastic moduli, at 15-km and 25-km depth, are marked with gray lines on the megathrust.

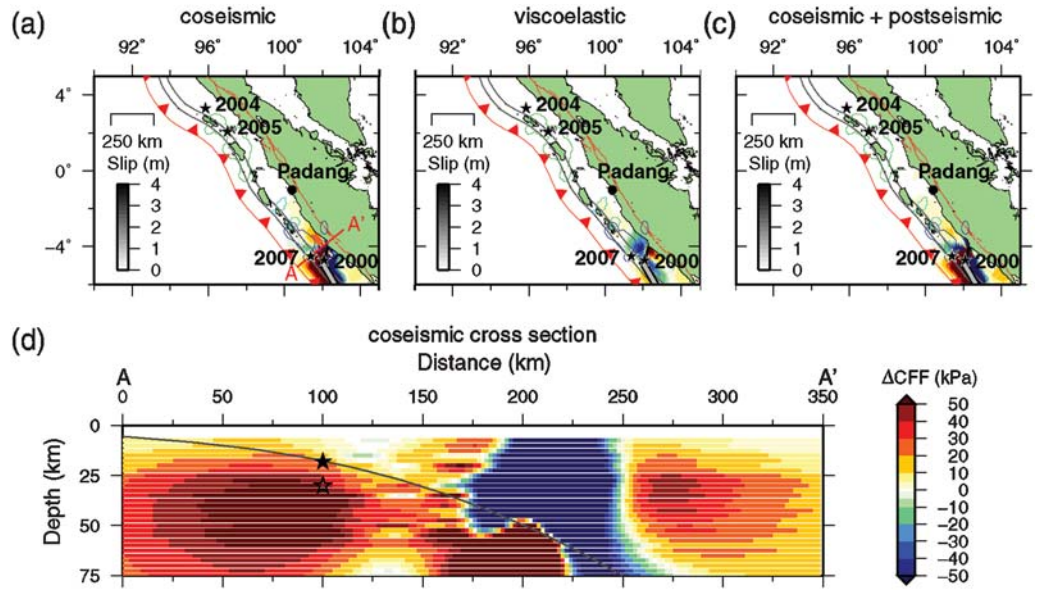

Figure 6. Coulomb failure stress changes on the Sunda megathrust resulting from the 2000 (a) coseismic deformation, (b) viscoelastic deformation, (c) total coseismic and postseismic (including poroelastic) deformation. The 2000 earthquake source model (Abercrombie *et al.*, 2003), 2005 slip contour (Konca *et al.*, 2007) and 2007 slip contours (Konca *et al.*, 2008) overlay the stress changes. The major increases in elastic moduli, at 15-km and 25-km depth, are marked with gray lines on the megathrust. (d) Cross section of coseismic CFF changes on megathrust parallel faults. The filled star marks the 2007 hypocenter for our preferred megathrust geometry and the open star marks the USGS hypocenter.

viscoelastic deformation relieved ~4 kPa of CFF (Fig. 6b) and brought the total CFF change to ~16 kPa at the time of the 2007 earthquake (Fig. 6c). Since the 2000 earthquake epicenter is only ~80 km southeast of the 2007 epicenter, variations in megathrust geometry can significantly impact the CFF changes in the 2007 hypocentral region. Figure 6d, a cross section of coseismic CFF changes on faults parallel to the megathrust from the trench to Sumatra and through the 2007 hypocenter, shows how the stress greatly increases below the megathrust. The coseismic CFF change increases from 18 kPa to 51 kPa, between the location of the 2007 earthquake on our preferred megathrust geometry and the USGS hypocenter. The total response, including coseismic and postseismic stress changes, varies between 16 kPa to 43 kPa.

By comparing the CFF changes at the 2007 hypocenter from the 2000, 2004, and 2005 earthquakes, it is evident that the 2000 event had the largest impact on the stress field. Figure 7 displays a time-series of the CFF changes at the 2007 hypocenter due to interseismic loading and the coseismic and postseismic CFF changes from the 2000, 2004, and 2005 earthquakes, relative to the state of stress at the beginning of 2000. The variability between the CFF change calculations at our preferred rupture depth and the USGS hypocenter is strongest for the 2000 coseismic response, but it is also evident in the viscoelastic decay following the 2000 and 2005 earthquakes. There is a larger positive coseismic CFF change at greater depths with an accompanying larger postseismic decay. The total coseismic and postseismic CFF changes from the 2000, 2004, and 2005 earthquakes is approximately equal to the interseismic loading between the 2000 and 2007 earthquakes for the USGS hypocenter, and approximately 1/2 the accumulated interseismic loading for our preferred hypocenter. Thus, although the 2000 earthquake provided the greatest triggering potential out of the three modeled earthquakes, it appears that the 2007 earthquake segment needed the additional loading provided by the seven years of interseismic stress accumulation.

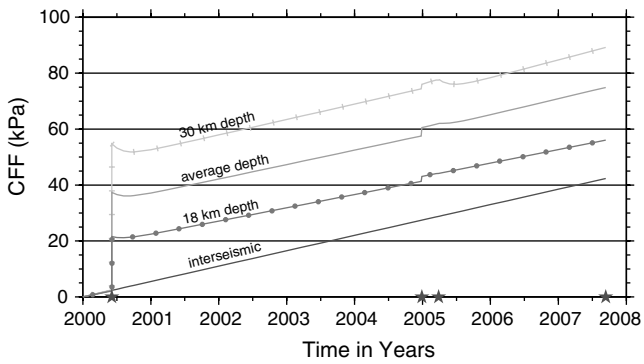

Figure 7. Accumulated CFF change at the 2007 hypocenter since the time of the 2000 earthquake. The CFF change is plotted for our preferred hypocentral depth on the plate-interface of 18 km, the USGS hypocentral depth of 30 km, and an average of the values between 18 km and 30 km depth. The accumulated CFF change includes coseismic and postseismic stress changes from the 2000, 2004, and 2005 earthquakes along with an interseismic stressing rate. Lacking knowledge of their time-dependence, the poroelastic and afterslip stress changes are added to the coseismic stress changes for the 2000, 2004, and 2005 earthquakes. The interseismic stressing rate is 5 kPa/yr at 18 km depth and 6 kPa/yr at 30 km depth. The average interseismic rate is plotted. The timing of the 2000, 2004, 2005, and 2007 earthquakes is marked with stars.

Seismicity Rate Comparison Method and Data

Seismicity Rate Change Calculation

We investigated seismicity changes following the 2004 earthquake using the standard beta-statistic approach (e.g., Hough, 2005; Reasenberg and Simpson, 1992). Beta is defined as $\beta = (N_a - N_e)/\text{sqrt(variance)}$, where N_a is the number of earthquakes in a given area occurring after a major event and N_e is the expected number of earthquakes based on preevent seismicity. Beta will be positive when the postseismic rate is higher than the background seismicity rate and negative when it is lower. We calculated β for 1-yr time intervals in 1° square cells. The preseismic period considered is between 1 January 1980 and 26 December 2004, but we also evaluate seismicity changes using a catalog ending in 1999, prior to the 2000 Enggano earthquake. The postseismic period starts on 26 December 2004, after the Sumatra–Andaman earthquake, and lasts until 12 September 2007.

Earthquake Catalog

Our earthquake catalog consists of the preferred events from IRIS SeismiQuery (see the Data and Resources section), with contributors limited to the International Seismological Center and the National Earthquake Information Service (Fig. 2b). The magnitude of completeness for the catalog, assuming a power law distribution of earthquakes with magnitude, is 4.7. For this rate comparison study, it is more important to have a larger number of earthquakes in the catalog than more precise locations. Therefore, we chose not to use the Engdahl relocated earthquake catalog (Engdahl *et al.*, 2007) in order to maximize the magnitude of completeness, and thereby the number of earthquakes in our catalog. Our catalog has a similar number of events as the Engdahl catalog at magnitudes greater than 5.0, but is more complete at lower magnitudes. We used ZMAP (Wiemer, 2001) to decluster the catalog in order to reduce the effect of aftershocks (for a comparison of the full catalog and declustered catalog, Ⓔ see Fig. S4 in the electronic supplement to this paper). The ZMAP declustering program uses Reasenberg's (1985) approach.

Seismicity Rate Comparison Results

In addition to modeling the static stress changes on the Sunda megathrust, we compare the level of seismicity before and after the 2004 earthquake to examine to what degree static and/or dynamic stress changes impacted seismicity rates along the Sunda subduction zone. Dynamic triggering induced by passing seismic waves can have a wider-reaching effect than static stress triggering (Freed, 2005 and references therein). Such dynamically triggered aftershocks can in turn trigger more earthquakes, including large ones (Felzer *et al.*, 2002). Increased levels of seismicity can also be associated with transient aseismic slip, as reflected in the apparent correlation of afterslip and aftershocks following the Nias earthquake (Hsu *et al.*, 2006). The distribution of the first nine months of Nias afterslip was strongly correlated with positive coseismic CFF changes on the plate-interface. This statically triggered aseismic slip may further stress the plate-interface, and therefore enable a delay time between the initial earthquake and a triggered event. Similarly, notable far-field seismicity increases could indicate the occurrence of a larger, dynamically triggered slow-slip transient.

Seismicity Rate Changes from 2005 to 2007

Figure 8 shows the β values for the years 2005–2007 in the Sumatra region, with the year 2004 until the Sumatra–Andaman earthquake also shown for comparison. In general, the seismicity level has been extremely elevated in western Sumatra and the offshore region north of the equator. The downdip width of the high-seismicity zone has narrowed each year since 2005, but seismicity levels still remain an order of magnitude higher in the 2004–2005 epicentral regions. In 2005, there was a vigorous cluster of aftershocks near Siberut Island, as evidenced by $\beta > 10$. From 2005 to 2007, there was a more moderate increase in seismicity in the region that slipped during the 2007 earthquake sequence, near the Mentawai Islands of Sipora, North Pagai, and South Pagai.

Seismicity in the 2007 Epicentral Region

In 2005, there were moderate seismicity increases of up to $\beta = 4$, in the 1° squares just north and south of the 2007 epicenter (Fig. 8b). There was a slight decrease in seismicity in the squares containing the 2007 and 2000 epicenters. In 2006, the seismicity increased to slightly positive in the 2007 and 2000 squares, but decreased in the surrounding region (Fig. 8c). The β values continued to decrease down to average levels during the first nine months of 2007 before the September earthquake (Fig. 8d).

When calculating β for the combined nine squares surrounding the 2007 epicenter, longitude 100°–103° and latitude 3° S–6° S, we see only small fluctuations in the pre-Enggano earthquake seismicity with a mean $\beta = -0.7$ and standard deviation of 0.8 for the years 1980–1999 (Fig. 9). The number of earthquakes increased greatly for the time period following the 2000 earthquake with a maximum $\beta \sim 10$; there was a second peak of moderate sized earthquakes from mid-2003 through 2004 (Figs. 8a, 9; for additional β value maps for 2000 to 2003, Ⓔ see Fig. S5 in the electronic supplement to this paper). The seismicity level quickly drops down to within 1-σ of the pre-2000 mean during 2005; however, the β values stay above the pre-2000 mean for 90% of the 2000–2007 time period. Overall, the seismicity levels are appreciably accelerated in the 2007 epicentral region following the 2000 Enggano earthquake with the increased seismicity levels decaying to near average rates by the time of the 2007 Bengkulu earthquake (for β value map using the 1980 to 1999 catalog, Ⓔ see Fig. S6 in the electronic supplement to this paper).

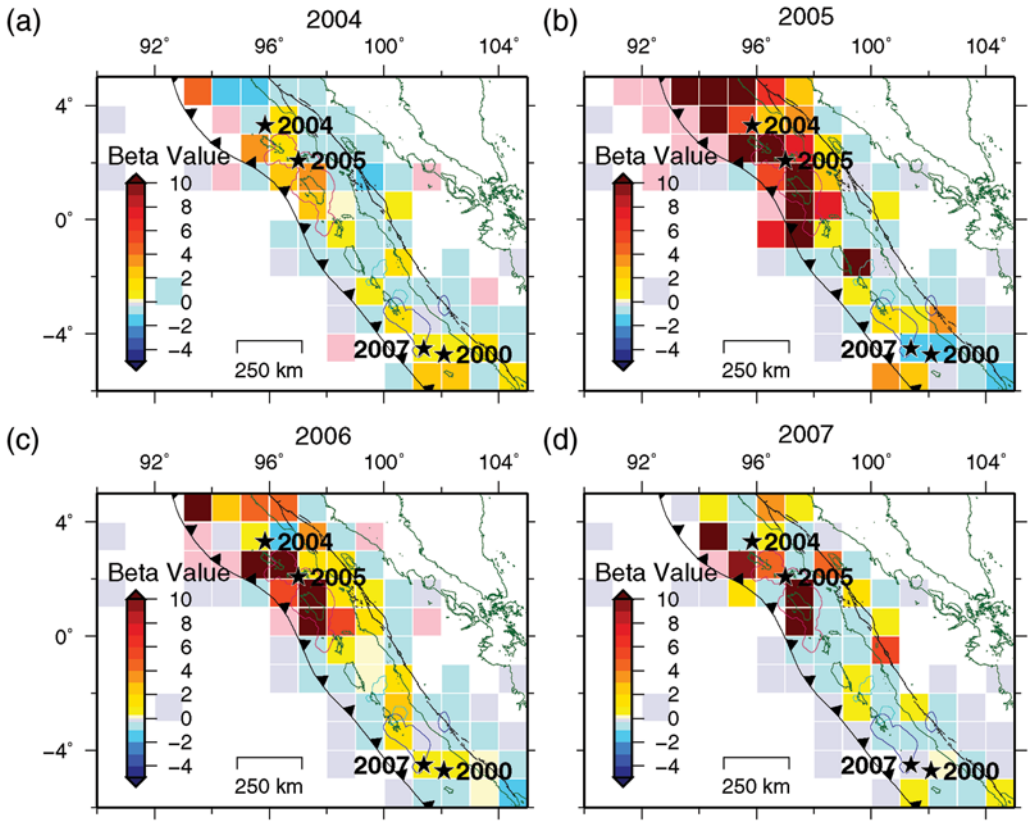

Figure 8. Beta values showing the relative change in seismicity following the 2004 earthquake compared with the time period 1980–2004. For the year: (a) 2004 (compared with 1980–2003), (b) 2005, (c) 2006, and (d) 2007 up to the September earthquake. The pink squares signify regions with earthquakes where there were no events during the preseismic period. The 2005 slip contour (Konca *et al.*, 2007) and 2007 slip contours (Konca *et al.*, 2008) overlay the beta values.

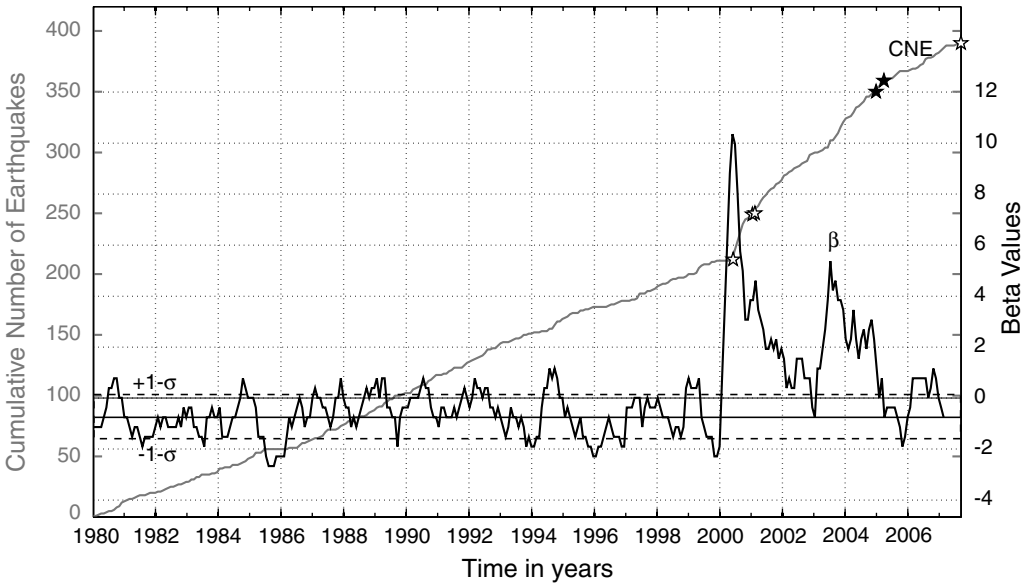

Figure 9. Beta values through time in a 3° × 3° area around the 2007 epicentral region are plotted with a thick line. The beta value is calculated for 0.5-yr time windows, with 30-day overlapping bins, and uses the declustered $M \geq 4.7$ catalog. In this case, each 0.5-yr interval (N_a) is compared with the entire 1980–2007 catalog (N_e). The cumulative number of earthquakes (CNE) since 1980 is plotted with a gray line. Earthquakes with $M \geq 6.5$ are marked with an open star, and the 2004 and 2005 earthquakes (not in the region) are marked with filled stars. A dashed rectangle encloses the mean ± 1-σ beta values based on years 1980–1999, before the 2000 Enggano earthquake.

Discussion

Differentiating Contributions from Different Postseismic Processes

There continues to be some uncertainty about the relative contributions from viscoelastic relaxation, afterslip, and poroelastic rebound to the deformation following the 2004 and 2005 earthquakes. Previous studies have fit the early postseismic geodetic data in the near field as afterslip updip and downdip from the main rupture patches (e.g., Hsu *et al.*, 2006; Paul *et al.*, 2007; Gahalaut *et al.*, 2008), whereas viscoelastic deformation is strongly indicated to dominate the far-field time-series (e.g., Pollitz, Bürgmann, and Banerjee, 2006; Pollitz *et al.*, 2008). Although all three postseismic processes are almost certain to be occurring during the time span between the 2004 and 2007, none of these mechanisms produce substantial stress changes at the 2007 hypocenter or elsewhere on its rupture zone.

Influence of Fault Friction

For this study, we assumed a weak megathrust with a low effective coefficient of friction, $\mu' = 0.1$. Cattin *et al.* (2009) analyzed the CFF and seismicity changes on faults adjacent to the Sunda megathrust, after the 2004–2005 earthquake sequence, as a way of estimating the effective coefficient of friction for nonmegathrust faults over a broad region from central Sumatra to southern Myanmar. Their analysis north of our study area, in the Andaman rift zone, strongly suggests that $\mu' > 0.5$ to explain the triggered seismicity there. They conclude that either the whole region has a high fault friction such as the Andaman rift zone, or there are significant spatial variations in the friction coefficient. Likewise, it is possible that there are variations in the friction coefficient along the megathrust, and we compare our results with models using $\mu' = 0.5$. We find that there are no defining differences in the 2007 hypocentral region due to the coseismic and postseismic CFF changes from the 2000, 2004, and 2005 earthquakes (Fig. 10c,d), as the large shear stress change overshadows the normal stress change (Fig. 10a, b). Interseismic creep at depth does impart a negative normal stress change on the shallower portions of the megathrust, therefore a smaller μ' would lead to larger CFF over time (Ⓔ see Fig. S7 in the electronic supplement to this paper for a stress timeline at the 2007 hypocenter using different values of μ'). Interestingly, when using $\mu' = 0.5$ there is

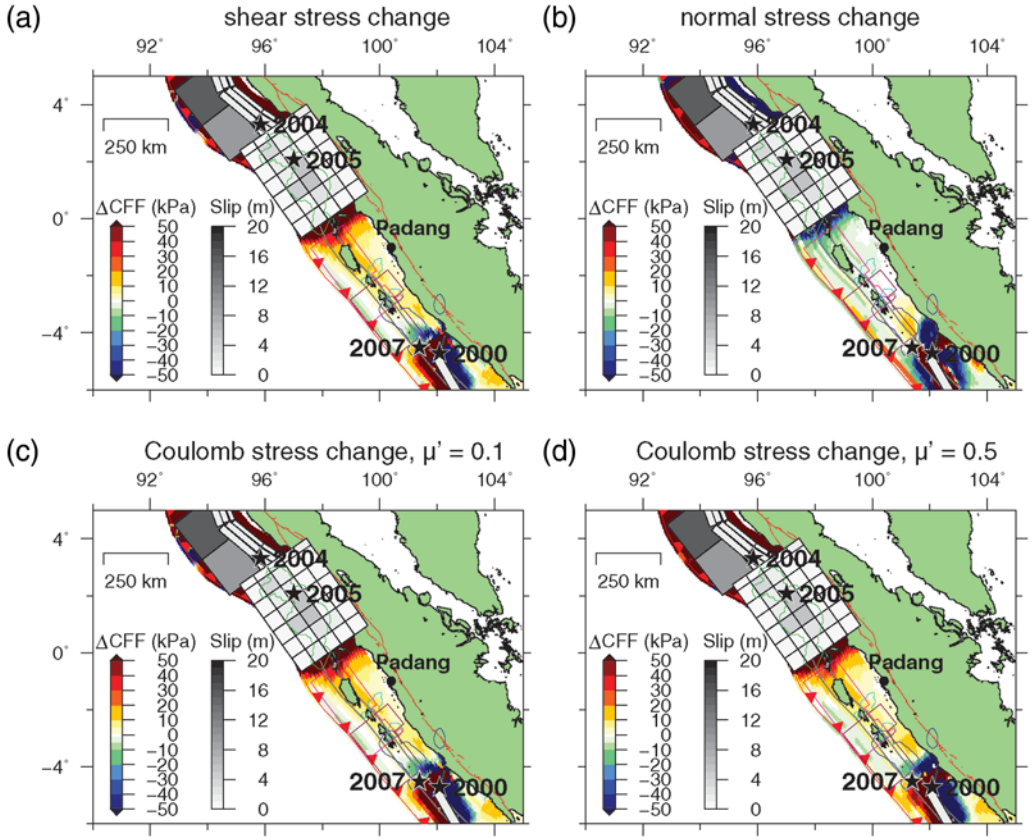

Figure 10. Total stress changes resulting from the combination of the 2000, 2004, and 2005 coseismic and postseismic deformation on the Sunda megathrust. Shown are (a) the shear stress component, (b) the normal stress component, (c) CFF with $\mu' = 0.1$, and (d) CFF with $\mu' = 0.5$. The earthquake source models (Abercrombie *et al.*, 2003; Banerjee *et al.*, 2007; Konca *et al.*, 2007), 2005 slip contour (Konca *et al.*, 2007), and 2007 slip contours (Konca *et al.*, 2008) overlay the stress changes. The 1797 and 1833 slip patches are also outlined (Natawidjaja *et al.*, 2006). The major increases in elastic moduli, at 15-km and 25-km depth, are marked with gray lines on the megathrust.

increased CFF change (up to 15 kPa) downdip of the 2007 main rupture patch, near the poorly resolved deep slip patch below the mainland of Sumatra.

The Skipped 1797 Rupture Patch

Again we pose the question, why did the 2007 earthquake rupture the southern portion of the 1833 rupture zone instead of rerupturing the historic 1797 rupture zone? Natawidjaja *et al.* (2006) found that the accumulated interseismic slip deficit since 1797 is greater than what was released during the earthquake, while the interseismic slip deficit accumulated over the 1833 segment has reached a maximum of 75% of the 1833 event slip. Total CFF changes since 2004 are positive and >10 kPa over the Siberut region in the northern half of the 1797 rupture zone. The total CFF changes are >10 kPa over a larger portion of the historic 1797 rupture segment than they are over the eventual 2007 rupture zone, which has a large positive value only near the hypocentral region (Fig. 10c).

However, the total normal stress changes are negative (clamping) over the 1797 rupture zone and positive over the 2007 rupture zone (Fig. 10b). This may indicate that the relatively small normal stress changes have a greater impact on triggered seismicity than is assumed by Coulomb failure theory. Similarly, Perfettini *et al.* (1999) observed an association between the peak slip locations from the 1989 Loma Prieta earthquake and portions of the fault that had been unclamped by the preceding Lake Elsman events. They suggest that the unclamping could have indirectly triggered the Loma Prieta earthquake by triggering aseismic creep. The periphery of the creep zone would sustain high shear stress increases, with the Loma Prieta hypocenter being located in this high stress region. Similarly, the 2000 earthquake unclamped the deeper half of the future 2007 rupture zone, which could have induced aseismic creep. A combination of coseismic CFF increases at the 2007 hypocenter from the 2000 earthquake and aseismic creep induced shear stress increases may explain why the southern 1833 segment ruptured before the 1797 segment.

Although previous studies have suggested that the 1797 earthquake had a smaller magnitude than the 1833 earthquake and has since accumulated a larger interseismic slip deficit, heterogeneities in the regional stress field may account for the southern initiation point of the 2007 earthquake. Slip distributions of the 1797 and 1833 earthquakes are not known in a detailed manner; it could be that in 1833 there was a relatively low-slip area over the future 2007 hypocentral region, and the positive CFF change imparted by the 2000 earthquake was enough to trigger the southern 1833 segment. Heterogeneities in the structure of the incoming oceanic crust may also affect the strength of the megathrust and the interseismic coupling rate and lead to a nonlinear relationship between the region with the largest CFF change and the locations of triggered events. One such crustal complexity is the Investigator Fracture Zone, which enters the Sunda trench in the region between the Batu Islands and Siberut, in the northernmost section of the 1797 rupture zone. This small section of the megathrust is likely poorly coupled (Chlieh *et al.*, 2008) and may explain why the 2005 earthquake did not trigger a large earthquake in this nearest, highly stressed portion of the Sunda megathrust. Nonetheless, the section just south of this poorly coupled segment, the Siberut segment, is strongly coupled, has not ruptured since 1797, has $\Delta\mathrm{CFF} > 10$ kPa from the 2005 earthquake, must be close to failure, and represents a substantial remaining earthquake and tsunami hazard in the region.

Delayed Dynamic Long-Distance Triggering

It is also possible that seismic waves could trigger aseismic slip episodes at large distances, and these slow-slip events can further stress the plate-interface and trigger additional earthquakes. One such far-field triggering example is the tremor triggered by teleseismic earthquakes in Cascadia, and the possible correlation between large teleseismic events and episodic tremor and slip episodes (Rubinstein *et al.*, 2009). Similarly, the 1992 Landers, California, earthquake was initiated by a swarm of foreshocks that appears to represent a slow-slip transient triggered by the preceding Joshua Tree earthquake (Dodge *et al.*, 1996). The observed increase in seismicity levels over the two eventual 2007 rupture zones during 2005 and 2006 (Fig. 8b,c), along with the increase in seismicity during the few years following the 2000 earthquake (Ⓔ Fig. S5a,b,c in the electronic supplement to this paper), may be evidence of such a delayed triggering mechanism. The increased level of moderate sized earthquakes could have promoted (or be a reflection of) aseismic creep over the portion of the 2007 rupture zone that was unclamped by the previous stress changes (Fig. 10b). Unfortunately, there is a lack of geodetic data during the two years following the 2000 earthquake; however, a comparison of GPS velocities for the years 1992–1994 and 2002–2007 at Enggano suggests a change in coupling of the plate-interface at this region south of the 2000 hypocenter (Prawirodirdjo *et al.*, 2010). Future analysis of the cGPS data spanning the time between the 2004 and 2007 earthquakes may be able to confirm whether there indeed was transient aseismic slip on this southern portion of the Sunda megathrust leading up to the two 2007 earthquakes.

Conclusions

Coulomb failure stress change at the 2007 M_w 8.4 hypocenter, resulting from the combined 2004–2005 coseismic and postseismic deformation, is likely too small to have triggered the recent earthquake. There are also no large negative CFF changes in the Siberut region from the combined 2004–2005 coseismic and postseismic deformations that could help explain the delayed recurrence of the 1797 earthquake. However, the normal stress change was negative

over the Siberut region and positive over the 2007 segment; this unclamping of the 2007 segment may have promoted an aseismic slip event and eventual rupture. The smaller 2000 Enggano earthquake turns out to have had the largest CFF change at the 2007 hypocenter and may help to explain its southern location. Investigations of seismicity rate changes across the region, for the years following the 2004 earthquake, show that there was increased seismic activity along the two 2007 rupture zones and overall higher levels of seismicity since the 2000 earthquake. Geodetic investigations are necessary to determine whether this increased level of seismicity was associated with accelerated aseismic slip on the Sunda megathrust, a potential contributing factor to the timing and location of the 2007 earthquake. Unfortunately, the earthquake and tsunami hazard still remains high for the Siberut region that last slipped in 1797.

Data and Resources

Earthquake location and magnitudes used in this study can be obtained from IRIS SeismiQuery at http://www.iris.washington.edu/SeismiQuery/sq-events.htm (last accessed 12 December 2007). The Global Centroid Moment Tensor Project database was searched using www.globalcmt.org/CMTsearch.html (last accessed 1 July 2008). Some plots were made using the Generic Mapping Tools version 4.1 (www.soest.hawaii.edu/gmt; Wessel and Smith, 1998).

Acknowledgments

This work is supported by the National Science Foundation grant EAR 0738299. We would like to thank Fred Pollitz for making his elastic and viscoelastic deformation software available to us and for providing helpful modeling suggestions. We would also like to thank Trey Apel for his insights throughout the duration of the project. Lastly we would like to thank Vineet Gahalaut and an anonymous reviewer for helpful suggestions that improved the manuscript. This is Berkeley Seismological Laboratory contribution 10-09.

References

Abercrombie, R. E., M. A. Antolik, and G. Ekstrom (2003). The June 2000 M_w 7.9 earthquakes south of Sumatra: Deformation in the India–Australia Plate, *J. Geophys. Res.* **108,** doi 10.1029/2001JB000674.

Aki, K. (1966). Generation and propagation of *G* waves from the Niigata earthquake of June 16, 1964. Part 2. Estimation of earthquake moment, released energy, and stress-strain drop from the *G* wave spectrum, *Bull. Earthquake Res. Inst., Tokyo Univ.* **44,** 73–88.

Banerjee, P., F. F. Pollitz, B. Nagarajan, and R. Bürgmann (2007). Coseismic slip distributions of the 26 December 2004 Sumatra–Andaman and 28 March 2005 Nias earthquakes from GPS static offsets, *Bull. Seismol. Soc. Am.* **97,** S86–S102.

Briggs, R. W., K. Sieh, A. J. Meltzner, D. Natawidjaja, J. Galetzka, B. Suwargadi, Y. Hsu, M. Simons, N. Hananto, I. Suprihanto, D. Prayudi, J. Avouac, L. Prawirodirdjo, and Y. Bock (2006). Deformation and slip along the Sunda megathrust in the great 2005 Nias–Simeulue earthquake, *Science* **311,** 1897–1901.

Cattin, R., N. Chamot-Rooke, M. Pubellier, A. Rabaute, M. Delescluse, C. Vigny, L. Fleitout, and P. Dubernet (2009). Stress change and effective friction coefficient along the Sumatra–Andaman–Sagaing fault system after the 26 December 2004 (M_w = 9.2) and the 28 March 2005 (M_w = 8.7) earthquakes, *G*^{3} **10,** doi 10.1029/2008GC002167.

Chlieh, M., J. Avouac, V. Hjorleifsdottir, T. A. Song, C. Ji, K. Sieh, A. Sladen, H. Hebert, L. Prawirodirdjo, Y. Bock, and J. Galetzka (2007). Coseismic slip and afterslip of the great Mw 9.15 Sumatra-Andaman earthquake of 2004, *Bull. Seismol. Soc. Am.* **97,** no. 1A, S152–S173.

Chlieh, M., J. P. Avouac, K. Sieh, D. H. Natawidjaja, and J. Galetzka (2008). Heterogeneous coupling of the Sumatran megathrust constrained by geodetic and paleogeodetic measurements, *J. Geophys. Res.* **113,** doi 10.1029/2007JB004981.

Curray, J. (2005). Tectonics and history of the Andaman Sea region, *J. Asian Earth Sci.* **25,** 187–232.

Dodge, D. A., G. C. Beroza, and W. L. Ellsworth (1996). Detailed observations of California foreshock sequences: Implications for the earthquake initiation process, *J. Geophys. Res.* **101,** 22,371–22,392.

Dziewonski, A. M., and D. L. Anderson (1981). Preliminary reference earth model, *Phys. Earth Planet. Int.* **25,** 297–356.

Engdahl, E. R., A. Villaseñor, H. R. DeShon, and C. H. Thurber (2007). Teleseismic relocation and assessment of seismicity (1918–2005) in the region of the 2004 M_w 9.0 Sumatra–Andaman and 2005 M_w 8.6 Nias Island great earthquakes, *Bull. Seismol. Soc. Am.* **97,** S43–S61.

Felzer, K. R., T. W. Becker, R. E. Abercrombie, G. Ekström, and J. R. Rice (2002). Triggering of the 1999 M_w 7.1 Hector Mine earthquake by aftershocks of the 1992 M_w 7.3 Landers earthquake, *J. Geophys. Res.* **107,** doi 10.1029/2001JB000911.

Fialko, Y. (2004). Evidence of fluid-filled upper crust from observations of postseismic deformation due to the 1992 M_w 7.3 Landers earthquake, *J. Geophys. Res.* **109,** doi 10.1029/2004JB002985.

Freed, A. M. (2005). Earthquake triggering by static, dynamic, and postseismic stress transfer, *Annu. Rev. Earth Planet. Sci.* **33,** 335–367.

Gahalaut, V. (2005). 28 March 2005 Sumatra earthquake: Expected, triggered or aftershock?, *Curr. Sci.* **89,** 452–454.

Gahalaut, V. K., S. Jade, J. K. Catherine, R. Gireesh, M. B. Ananda, P. Dileep Kumar, M. Narsaiah, S. S. H. Jafri, A. Ambikapathy, A. Bansal, R. K. Chadha, D. C. Gupta, B. Nagarajan, and S. Kumar (2008). GPS measurements of postseismic deformation in the Andaman–Nicobar region following the giant 2004 Sumatra–Andaman earthquake, *J. Geophys. Res.* **113,** doi 10.1029/2007JB005511.

Goldfinger, C., K. Grijalva, R. Bürgmann, A. E. Morey, J. E. Johnson, C. H. Nelson, J. Gutiérrez-Pastor, A. Ericsson, E. Karabanov, J. D. Chaytor, J. Patton, and E. Grácia (2008). Late Holocene rupture of the Northern San Andreas Fault and possible stress linkage to the Cascadia subduction zone, *Bull. Seismol. Soc. Am.* **98,** 861–889.

Hough, S. E. (2005). Remotely triggered earthquakes following moderate mainshocks (or, why California is not falling into the ocean), *Seismol. Res. Lett.* **76,** 58–66.

Hsu, Y., M. Simons, J. Avouac, J. Galetzka, K. Sieh, M. Chlieh, D. Natawidjaja, L. Prawirodirdjo, and Y. Bock (2006). Frictional afterslip following the 2005 Nias–Simeulue earthquake, Sumatra, *Science* **312,** 1921–1926.

Konca, A. O., J. Avouac, A. Sladen, A. J. Meltzner, K. Sieh, P. Fang, Z. Li, J. Galetzka, J. Genrich, M. Chlieh, D. H. Natawidjaja, Y. Bock, E. J. Fielding, C. Ji, and D. V. Helmberger (2008). Partial rupture of a locked patch of the Sumatra megathrust during the 2007 earthquake sequence, *Nature* **465,** 631–635.

Konca, A. O., V. Hjorleifsdottir, T. A. Song, J. Avouac, D. V. Helmberger, C. Ji, K. Sieh, R. Briggs, and A. Meltzner (2007). Rupture kinematics of the 2005 M_w 8.6 Nias–Simeulue earthquake from the joint inversion of seismic and geodetic data, *Bull. Seismol. Soc. Am.* **97,** S307–S322.

Lin, J., and R. S. Stein (2004). Stress triggering in thrust and subduction earthquakes and stress interaction between the southern San Andreas and nearby thrust and strike-slip faults, *J. Geophys. Res.* **109,** doi 10.1029/2003JB002607.

Masterlark, T. (2003). Finite element model predictions of static deformation from dislocation sources in a subduction zone: Sensitivities to homogenous isotropic, Poisson-solid, and half-space assumptions, *J. Geophys. Res.* **108,** doi 10.1029/2002JB002296.

Masterlark, T., C. DeMets, H. F. Wang, O. Sánchez, and J. Stock (2001). Homogeneous vs heterogeneous subduction zone models: Coseismic and postseismic deformation, *Geophys. Res. Lett.* **28,** 4047–4050.

McCloskey, J., S. S. Nalbant, and S. Steacy (2005). Earthquake risk from co-seismic stress, *Nature* **434,** 291.

Nalbant, S. S., S. Steacy, K. Sieh, D. Natawidjaja, and J. McCloskey (2005). Earthquake risk on the Sunda trench, *Nature* **435,** 756–757.

Natawidjaja, D. H., K. Sieh, M. Chlieh, J. Galetzka, B. W. Suwargadi, H. Cheng, R. L. Edwards, J. Avouac, and S. N. Ward (2006). Source parameters of the great Sumatran megathrust earthquakes of 1797 and 1833 inferred from coral microatolls, *J. Geophys. Res.* **111,** doi 10.1029/2005JB004025.

Ogawa, R., and K. Heki (2007). Slow postseismic recovery of geoid depression formed by the 2004 Sumatra–Andaman earthquake by mantle water diffusion, *Geophys. Res. Lett.* **34,** doi 10.1029/2007GL029340.

Paul, J., A. R. Lowry, R. Bilham, S. Sen, and R. Smalley Jr. (2007). Postseismic deformation of the Andaman Islands following the 26 December, 2004 Great Sumatra–Andaman earthquake, *Geophys. Res. Lett.* **34,** doi 10.1029/2007GL031024.

Pollitz, F. F. (1992). Postseismic relaxation theory on the spherical earth, *Bull. Seismol. Soc. Am.* **82,** 422–453.

Pollitz, F. F. (1996). Coseismic deformation from earthquake faulting on a layered spherical earth, *Geophys. J. Int.* **125,** 1–14.

Pollitz, F. F., P. Banerjee, R. Bürgmann, M. Hashimoto, and N. Chhoosakul (2006). Stress changes along the Sunda trench following the 26 December 2004 Sumatra–Andaman and 28 March 2005 Nias earthquakes, *Geophys. Res. Lett.* **33,** doi 10.1029/2005GL024558.

Pollitz, F. F., R. Bürgmann, and P. Banerjee (2006). Post-seismic relaxation following the great 2004 Sumatra–Andaman earthquake on a compressible self-gravitating Earth, *Geophys. J. Int.* **167,** 397–420.

Pollitz, F., P. Banerjee, K. Grijalva, B. Nagarajan, and R. Bürgmann (2008). Effect of 3-D viscoelastic structure on post-seismic relaxation from the 2004 $M = 9.2$ Sumatra earthquake, *Geophys. J. Int.* **173,** doi 10.1111/j.1365-246X.2007.03666.x.

Perfettini, H., R. S. Stein, R. Simpson, and M. Cocco (1999). Stress transfer by the 1988–1989 $M = 5.3$ and 5.4 Lake Elsman foreshocks to the Loma Prieta fault: Unclamping at the site of peak mainshock slip, *J. Geophys. Res.* **104,** 20,169–20,182.

Prawirodirdjo, L., R. McCaffrey, C. D. Chadwell, Y. Bock, and C. Subarya (2010). Geodetic observations of an earthquake cycle at the Sumatra subduction zone: Role of interseismic strain segmentation, *J. Geophys. Res.* **115,** doi 10.1029/2008JB006139.

Reasenberg, P. (1985). Second-order moment of central California seismicity, 1969–1982, *J. Geophys. Res.* **90,** 5479–5495.

Reasenberg, P. A., and R. W. Simpson (1992). Response of regional seismicity to the static stress change produced by the Loma Prieta earthquake, *Science* **255,** 1687–1690.

Rubinstein, J. L., J. Gomberg, J. E. Vidale, A. G. Wech, H. Kao, K. C. Creager, and G. Rogers (2009). Seismic wave triggering of nonvolcanic tremor, ETS, and earthquakes on Vancouver Island, *J. Geophys. Res.* **114,** doi 10.1029/2008JB005875.

Rydelek, P. A., and I. S. Sacks (1999). Large earthquake occurrence affected by small stress changes, *Bull. Seismol. Soc. Am.* **89,** 822–828.

Shearer, P., and R. Bürgmann (2010). Lessons learned from the 2004 Sumatra–Andaman megathrust rupture, *Annu. Rev. Earth Planet. Sci.* **38**, 103–131.

Sieh, K., D. H. Natawidjaja, A. J. Meltzner, C. Shen, H. Cheng, K. Li, B. W. Suwargadi, J. Galetzka, B. Philibosian, and R. L. Edwards (2008). Earthquake supercycles inferred from sea-level changes recorded in the corals of West Sumatra, *Science* **322,** 1674–1678.

Subarya, C., M. Chlieh, L. Prawirodirdjo, J. Avouac, Y. Bock, K. Sieh, A. J. Meltzner, D. H. Natawidjaja, and R. McCaffrey (2006). Plate-boundary deformation associated with the great Sumatra–Andaman earthquake, *Nature* **440,** 46–51.

Suppe, J. (2007). Absolute fault and crustal strength from wedge tapers, *Geology* **35,** 1127–1130.

Toda, S., R. S. Stein, K. Richards-Dinger, and S. B. Bozkurt (2005). Forecasting the evolution of seismicity in southern California: Animations built on earthquake stress transfer, *J. Geophys. Res.* **110,** doi 10.1029/2004JB003415.

Wang, K., and J. He (1999). Mechanics of low-stress forearcs: Nankai and Cascadia, *J. Geophys. Res.* **104,** 15,191–15,205.

Wang, K., T. Mulder, G. C. Rogers, and R. D. Hyndman (1995). Case for very low coupling stress on the Cascadia subduction fault, *J. Geophys. Res.* **100,** 12,907–12,918.

Wessel, P., and W. H. Smith (1998). New, improved version of the Generic Mapping Tools released, *Eos Trans. AGU* **79,** 579.

Wiemer, S. (2001). A software package to analyze seismicity: ZMAP, *Seismol. Res. Lett.* **72,** 373–382.

Zhou, Y. H., L. S. Xu, and Y. T. Chen (2002). Source process of the 4 June 2000 southern Sumatra, Indonesia, earthquake, *Bull. Seismol. Soc. Am.* **92,** 2027–2035.

Department of Earth and Planetary Science
University of California, Berkeley
307 McCone Hall
Berkeley, California 94720-4767
kelly@seismo.berkeley.edu

Manuscript received 18 March 2010

Supplementary Material

The supplementary material includes figures of coseismic stress changes with variable fault geometry (Figure S1), interseismic stress change (Figure S2), poroelastic stress change from the 2000 earthquake with variable fluid saturation depths (Figure S3), earthquake catalog histograms (Figure S4), seismicity rate change from different time periods (Figure S5 & S6), and stress changes at 2007 hypocenter using variable fault friction (Figure S7).

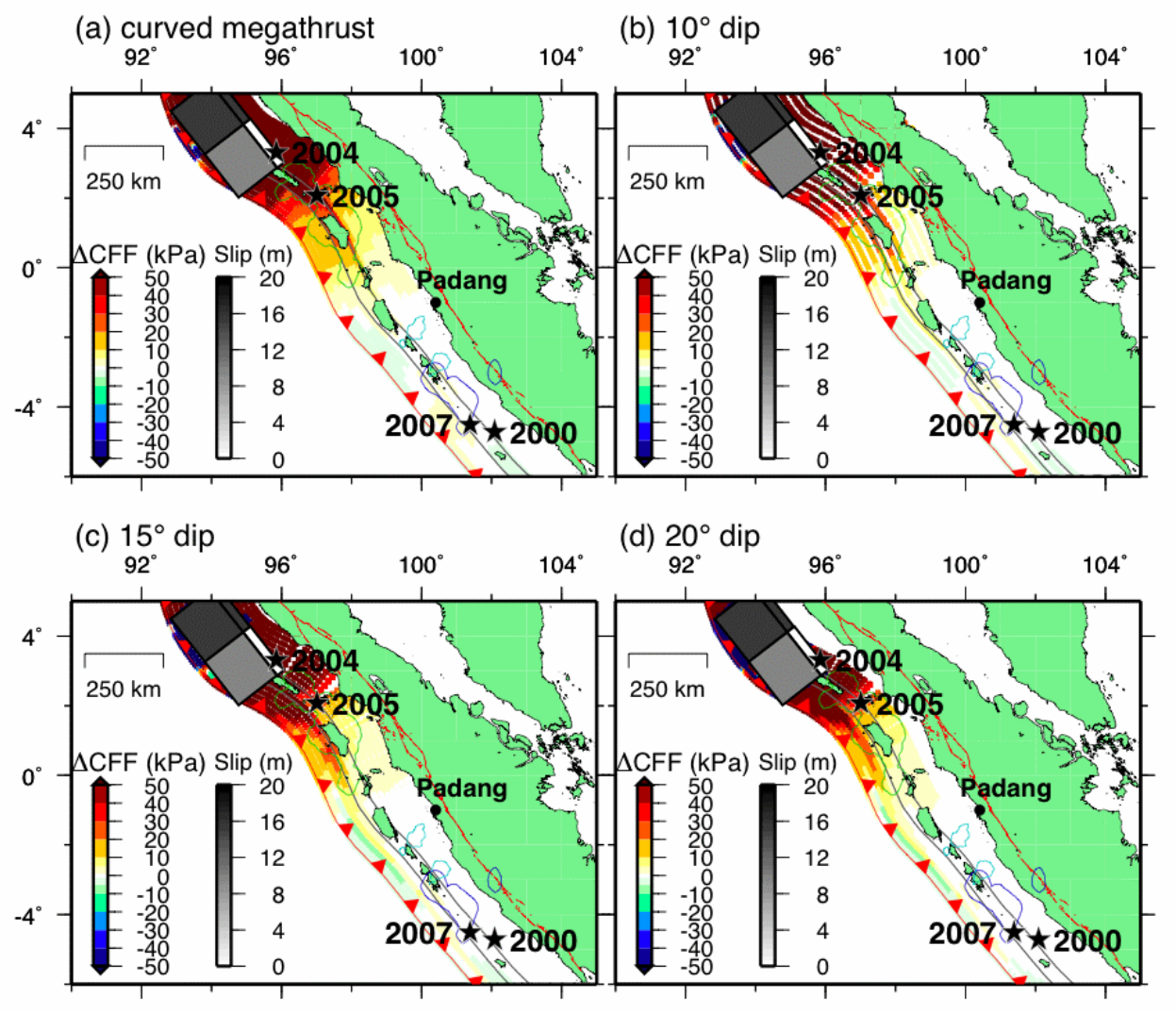

Figure S1. Sumatra coseismic CFF change resolved on a) preferred curved megathrust, b) 10° dipping plane, c) 15° dipping plane, and d) 20° dipping plane. All of the CFF maps cover the same depth range. The main difference between the varied models is the location of the high stress region that extends past Siberut. This increase in CFF change is due to the increase in elastic stiffness parameters at 15 km and 25 km depth and the downdip edge of the rupture at 30 km depth. The geometrical differences insubstantially impact the CFF change values at the deeper portions of the megathrust, at depths greater than the source model.

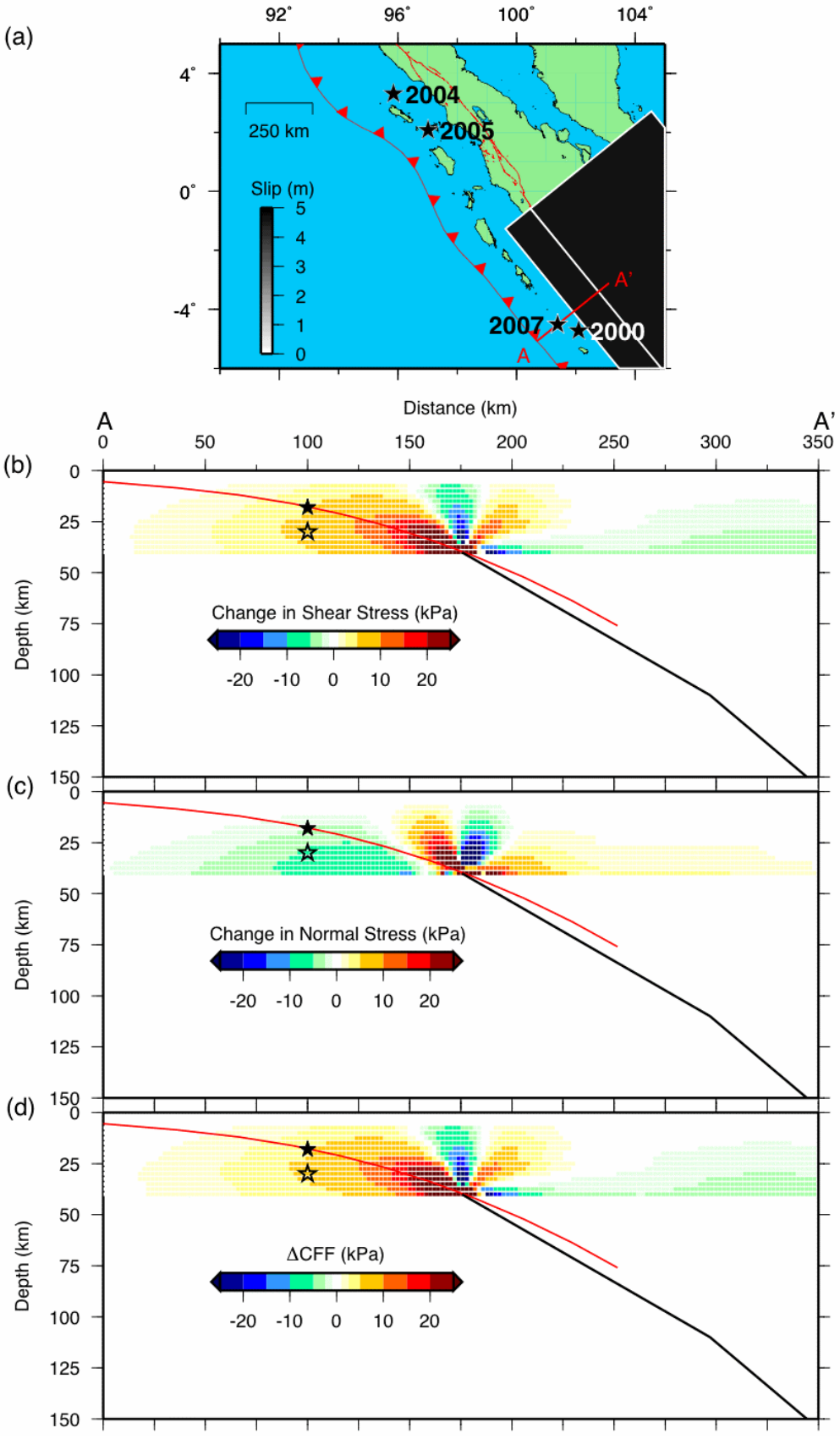
(a)
92°
96°
100°
104°
4°
0°
-4°
2004
2005
2007
2000
250 km
Slip (m)
5
4
3
2
1
0
A
A'
Distance (km)
A
A'
0
50
100
150
200
250
300
350
(b)
Depth (km)
Change in Shear Stress (kPa)
-20
-10
0
10
20
(c)
Change in Normal Stress (kPa)
(d)
ΔCFF (kPa)

Figure S2. Two-plane interseismic model for the 2007 hypocentral region. a) The two-plane interseismic model approximates the geometry of the curved megathrust with plane-1 extending from 40 to 110 km depth at a 30° dip and plane-2 extending from 110 to 600 km depth at a 40° dip. Both planes have a uniform 4.5 cm/yr reverse slip and extend along strike for 800 km. Interseismic annual stressing rates are shown at cross section A-A' for b) shear stress, c) normal stress, and d) CFF with μ' = 0.1. The black planes are the source faults and the red planes are the receiver fault (preferred megathrust geometry). The 2007 hypocenter on our preferred megathrust geometry is shown by a filled star and the USGS hypocenter is shown by an open star. The CFF change is 5 kPa/year at our preferred hypocenter and 6 kPa/year at the USGS hypocenter.

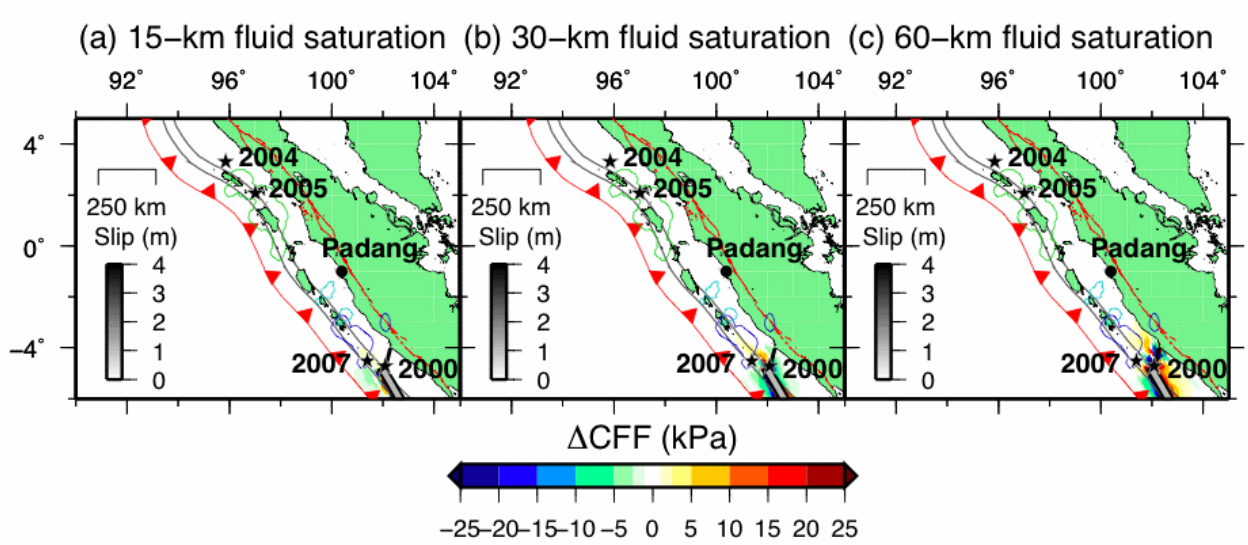

Figure S3. 2000 poroelastic CFF change model for a) pore-fluid saturation down to 15-km depth, b) pore-fluid saturation down to 30-km depth, and c) pore-fluid saturation down to 60-km depth. Although the extent of the large poroelastic CFF changes increases with increased pore-fluid saturation depth, the 2007 hypocenter is too distant to be sensitive to these changes.

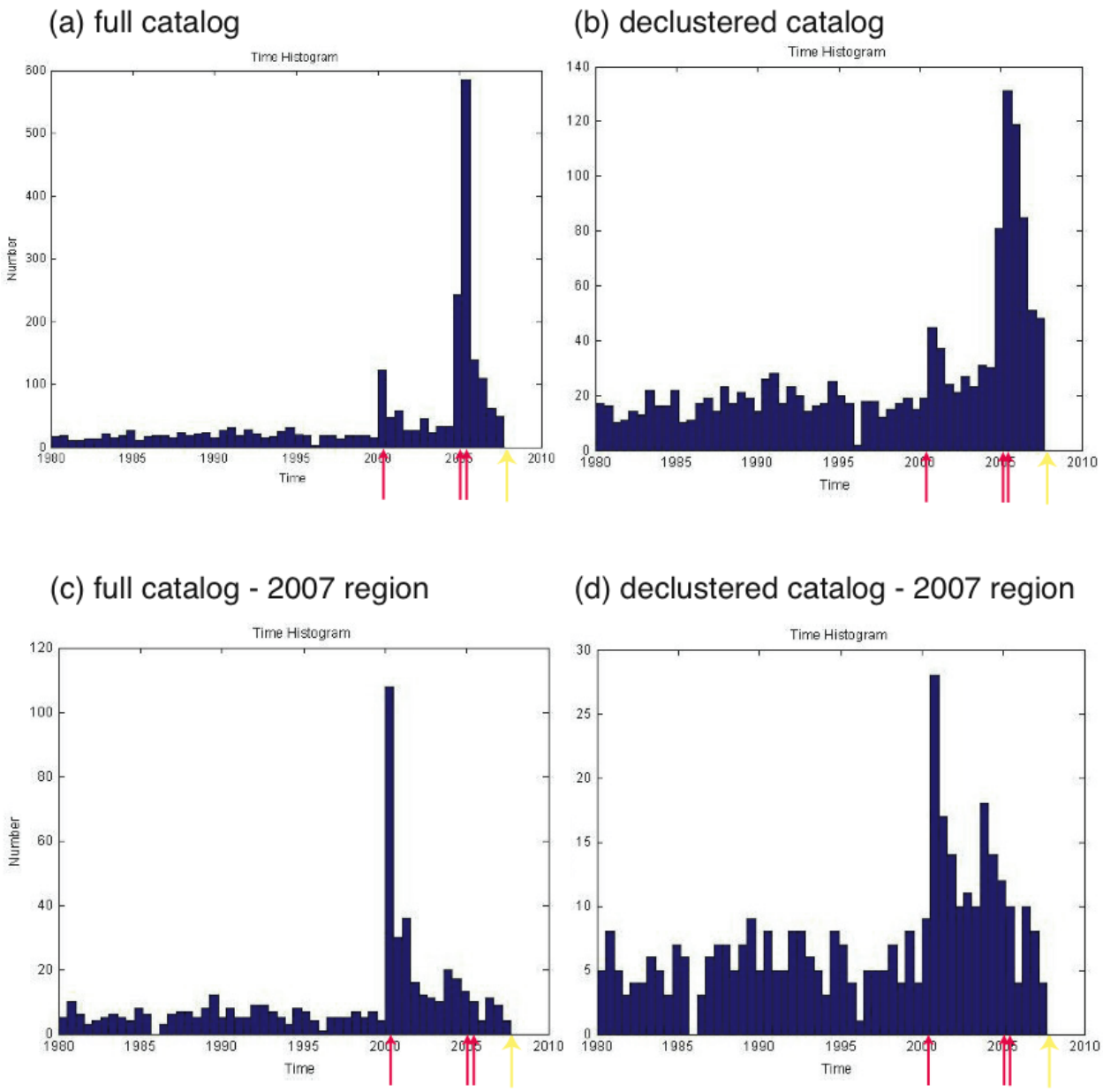

Figure S4. M ≥ 4.7 and depth < 100 km seismicity from a) full catalog, b) declustered catalog, c) catalog restricted to 2007 epicentral region, and d) declustered catalog restricted to 2007 epicentral region. The red arrows point to the 2000, 2004, and 2005 earthquakes and the yellow arrow points to the 2007 earthquake.

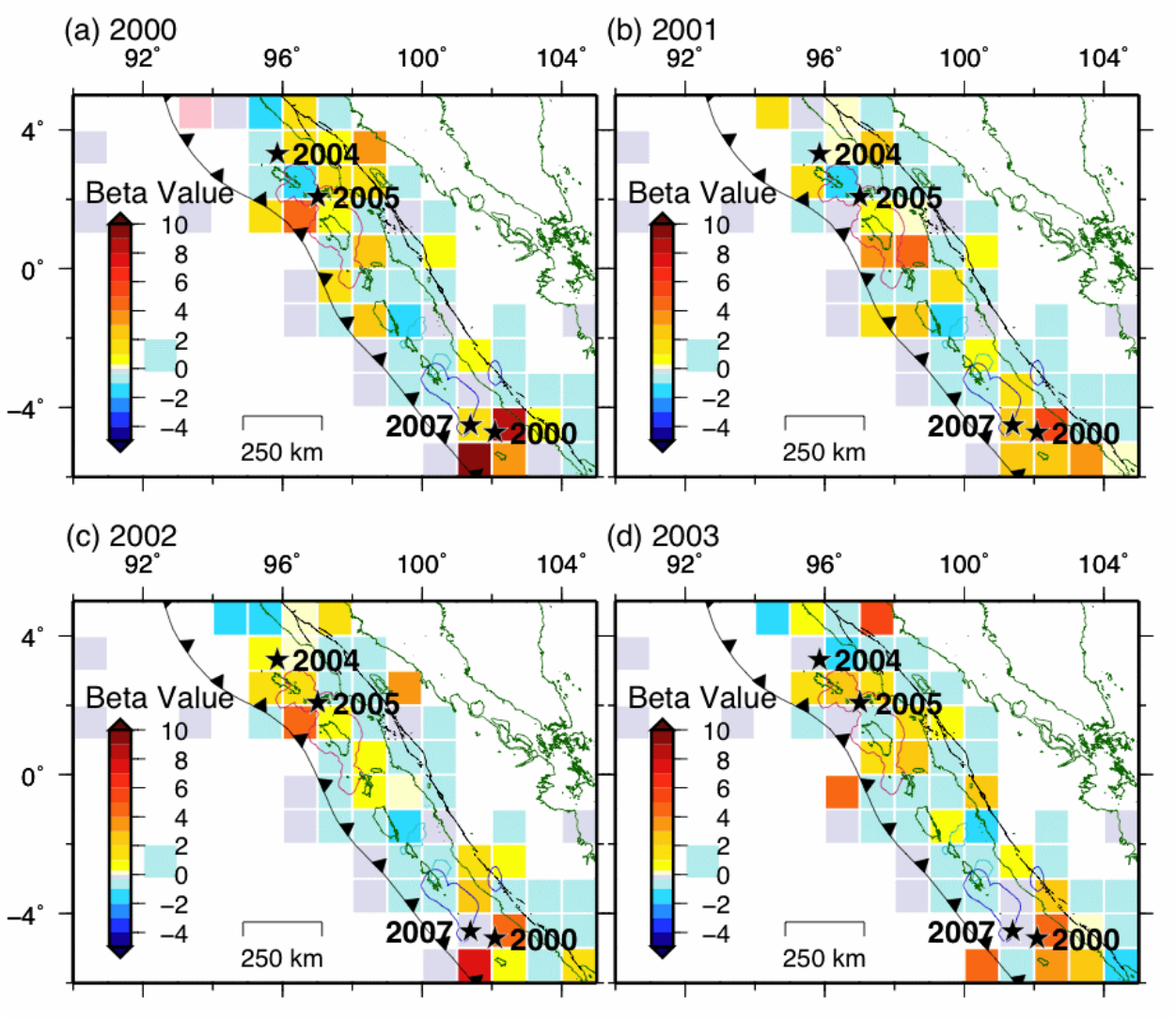

Figure S5. Beta values showing the relative change in seismicity compared to the time period 1980-1999. For the year: a) 2000, b) 2001, c) 2002, and d) 2003. The pink squares signify regions with aftershocks where there were no earthquakes during the preseismic period. The 2005 slip contour (Konca *et al.*, 2007) and 2007 slip contours (Konca *et al.*, 2008) overlay the beta values.

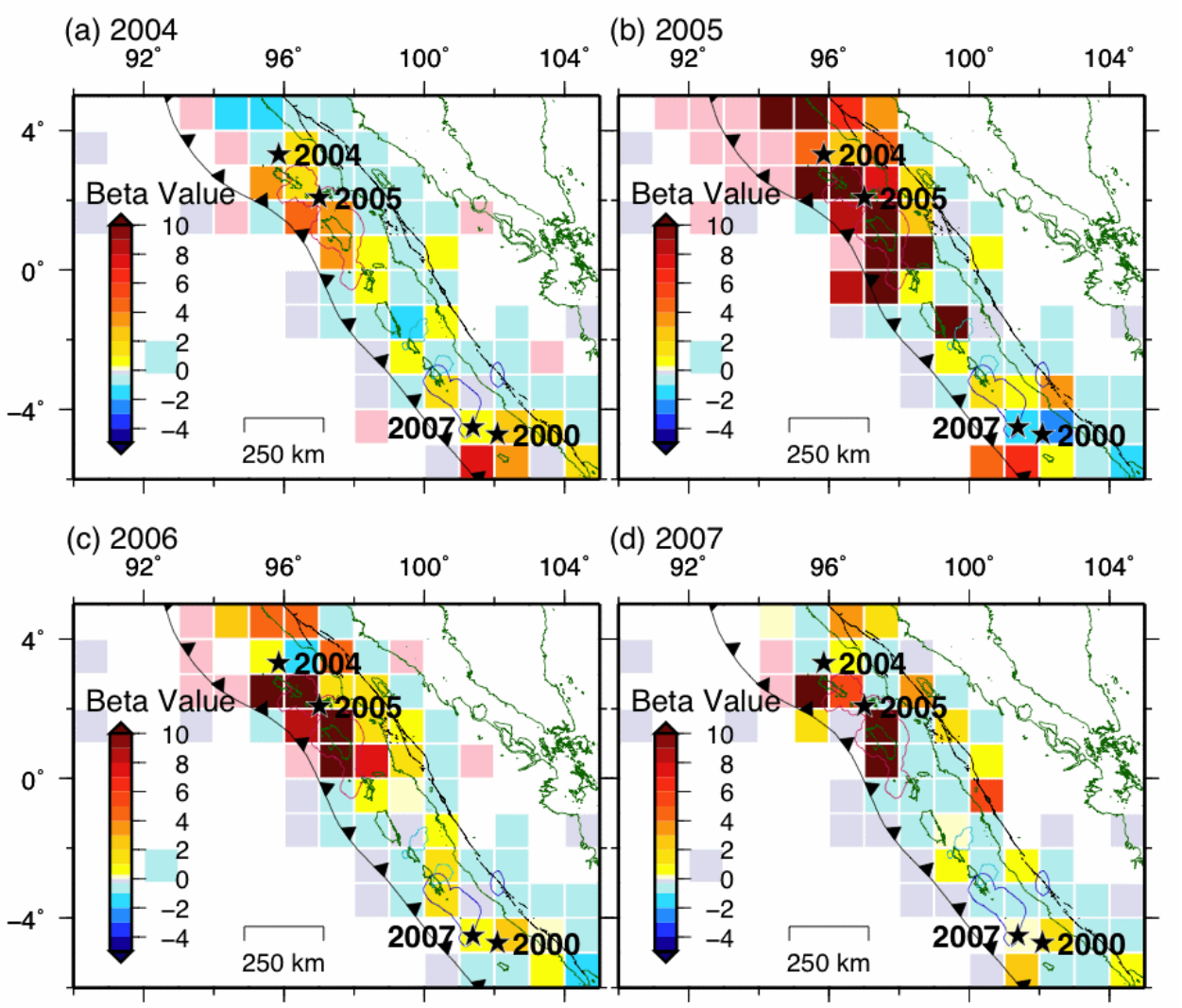

Figure S6. Beta values showing the relative change in seismicity compared to the time period 1980-1999. For the year: a) 2004, b) 2005, c) 2006, and d) 2007 up to the September earthquake. The pink squares signify regions with aftershocks where there were no earthquakes during the preseismic period. The 2005 slip contour (Konca *et al.*, 2007) and 2007 slip contours (Konca *et al.*, 2008) overlay the beta values.

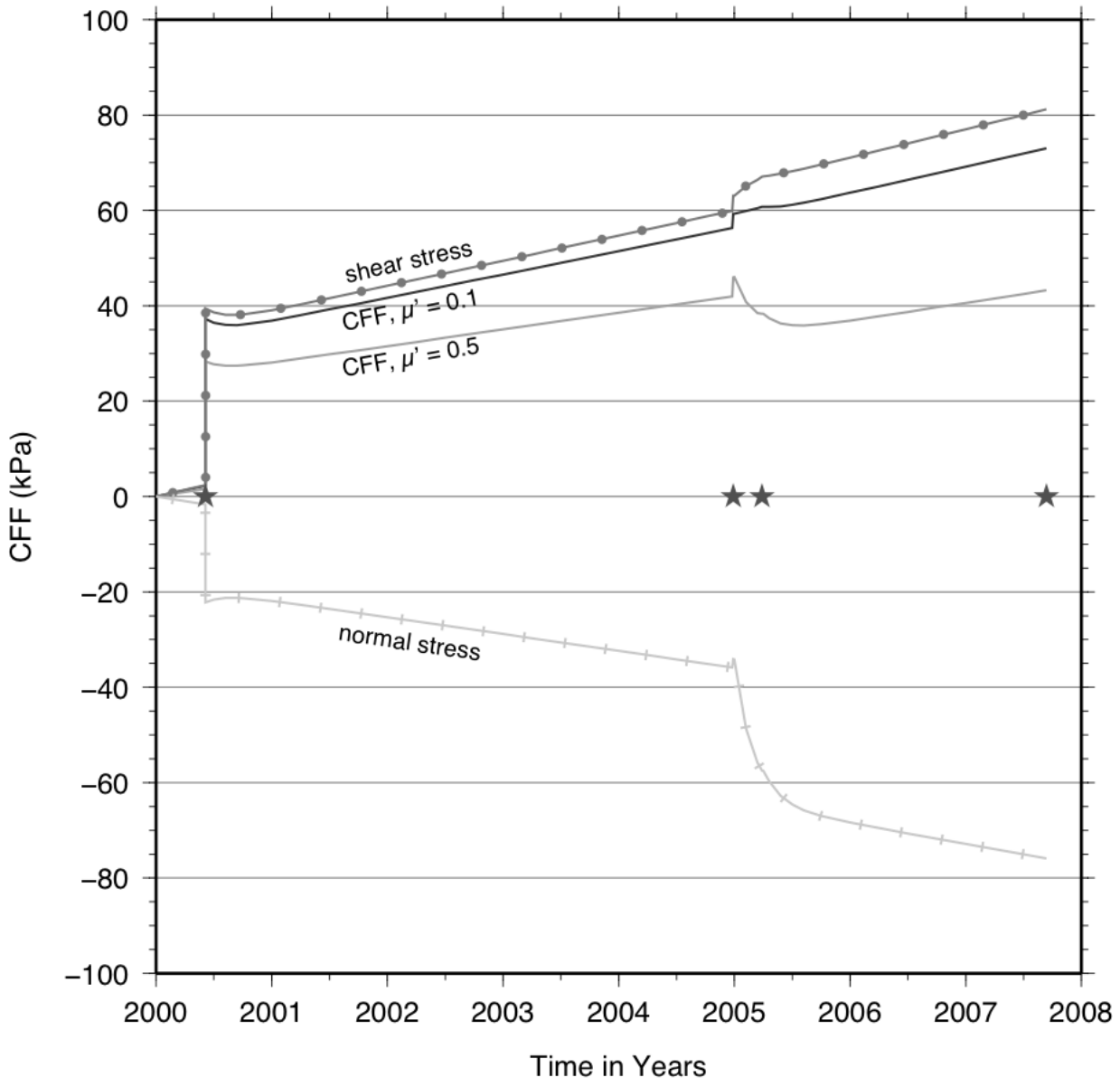

Figure S7. Accumulated stress change at the 2007 hypocenter since the time of the 2000 earthquake. The normal stress change, shear stress change, and CFF change (μ' = 0.1 and 0.5) is plotted at the average hypocentral depth (between our 18 km depth and the USGS 30 km depth). The accumulated CFF change includes coseismic and postseismic stress changes from the 2000, 2004, and 2005 earthquakes along with an interseismic stressing rate. Lacking knowledge of their time-dependence, the poroelastic and afterslip stress changes are added to the coseismic stress changes for the 2000, 2004, and 2005 earthquakes. The timing of the 2000, 2004, 2005, and 2007 earthquakes are marked with stars.